



THE MINISTRY OF NATIONAL INFRASTRUCTURES
GEOLOGICAL SURVEY OF ISRAEL

Israel Geodynamic Radon Project

Experimental replication of radon signals that occur in the geological environment

G. Steinitz, O. Piatibratova





THE MINISTRY OF NATIONAL INFRASTRUCTURES
GEOLOGICAL SURVEY OF ISRAEL

Israel Geodynamic Radon Project

**Experimental replication of radon signals that occur
in the geological environment**

G. Steinitz, O. Piatibratova

Jerusalem, July, 2008

Report GSI/17/2008

Contents

Abstract	
Introduction	1
Experiment Phases and Stages	2
Experimental Setup.....	3
Radiation Detectors	5
Data Collection and Pre-Processing	6
Additional Measurements and Complementary Investigations	6
Results.....	7
Signal Patterns	7
Environmental Influences	14
Daily Variations	17
Daily Amplitude (DA)	17
Periodicity - Daily Radon (DR) Signals	18
Temporal Patterns in the Periodic Characteristics of the DR Signal.....	19
The External Gamma Radiation Pattern – Complementary Investigations (CI).....	21
Discussion	39
Implications.....	43
Acknowledgements	43
References	44

List of Figures

Figure 1: Experimental layout showing the tank with the phosphorite, the internal gamma and alpha sensors and the position of the two external lateral gamma sensors. Gamma-C is immersed within a lead tube (0.5 cm thick). The radiation shield in front of gamma-E is also indicated. DL – data logger.	4
Figure 2: The experimental setup. A – Front view of tank with indication (horizontal mark) of internal phosphorite level. Three radiation sensors are inserted from the top; B – tank with upper planks removed; C – central plank with tubes for inserting sensors. Sensors are inserted with gaskets.	4
Figure 3: The daily average radiation registered by the internal radiation detectors	7
Figure 4: Correlations of daily average among the alpha detectors, during and following the initial build-up of radon in the tank	8
Figure 5: Time series of the daily average in the plateau interval (following initial build-up from Day 5503 to 5525) as recorded by the three internal radiation detectors.....	9
Figure 6: A 170-day long segment of the smoothed time series of the internal radiation detectors showing a multi-day (MD) variation. Different co-variation patterns are observed among the sensors. See text.	10
Figure 7: Detail of Figure 6 showing corresponding MD patterns among all three sensors. See text.	10
Figure 8: Detail of Figure 6 showing matching MD patterns among the two alpha detectors and a dissimilar variation pattern of the gamma-C. Time lags of up to few days of the MD signal occur between the alpha detectors. See text.	11
Figure 9: A 70-day long segment of the measured signal recorded by the internal radiation sensors showing the multi-day (MD) and diurnal radon (DR) variation. MD signals are recorded by the three sensors and DR signals, having different appearance, are dominating the time series of alpha-H and gamma-C.	12
Figure 10: The daily variation of the radiometric signal in the tank, extracted as the residual of the 25-hour smoothing. Different relative scales and different DR patterns characterize the signal of each sensor. See text.	12
Figure 11: 10-day detail of Figure 10 showing the DR signals recorded by the internal radiometric sensors. A DR signal is barely observable at alpha-L. Large but highly differing DR signals, primarily in phase, are recorded by alpha-H and gamma-C. The daily cycle dominates, but a semi-diurnal component is clearly observable in the gamma-C signal. The relatively low S/N signal of the alpha detectors does not enable distinguishing a semi-diurnal component in them.	13
Figure 12: Dependence of pressure inside the tank on the external ambient air pressure. Hourly averages in Days 3680-3739.	14
Figure 13: Relation between hourly averages of the radiation level at gamma-C sensor and pressure (left), and temperature (right).	15

Figure 14: Pressure (A) and temperature (B) variation inside the tank. Each time series is shown decomposed (using a 25-hour sliding average) to the periodic daily variation and the longer term variation. The longer term variations are used in Figure 15.....	15
Figure 15: The longer term variation the alpha and gamma radiation inside the tank and the concurrent long term variation of internal pressure (A) and temperature (B). See text.....	16
Figure 16: Temporal variation of the Daily Amplitude (DA) of the measured radon signal. See text.....	17
Figure 17: Spectra (FFT) of the time series (measured signal; 1-hour resolution) recorded by the internal sensors in the time interval of Days 5525-5950. Frequencies typical of S1, S2 and S3 periodicities occur in the diurnal band, exhibiting different relative amplitudes among the sensors. See text.	18
Figure 18: The temporal variation of amplitude (left) and phase (right) of the periodic DR signal measured by the internal radiation sensors. See text.....	20
Figure 19: Time series of daily averages (DM) of the internal and external (lateral) gamma sensors. The time intervals of complementary investigations (CI) are indicated. See Table 3 and text.....	21
Figure 20: Influence on gamma-C of an external gamma source placed at different levels of the tank (squares).	22
Figure 21: Influence of an external gamma source at 10 cm, activated between 14:00-15:20 hours, on the count rate of gamma-C. Sampling is at 1-minute resolution; Dots indicate the 15-minute readings.	23
Figure 22: Layout of experimental monitoring at the phosphorite level (10 cm from bottom of tank). The zone of gamma-rays originating from the phosphorite and influencing the detector is shown, based on Figure 21. See text.	24
Figure 23: A 15-day record of a gamma sensor placed outside and next to the tank at a level of 10cm. Pb bricks (Figure 22) shield the sensor from gamma radiation originating in the air volume of the tank.	25
Figure 24: Time series from the lateral gamma detectors showing: a) similar overall levels; b) superimposed periodic Daily Radon (DR) signals and c) non-periodic short Sub Diurnal Radon (SDR) signals. The concurrent time series of gamma-C is also shown, exhibiting DR signals with $\times 10$ amplitudes. MD signals are apparent only in the record of gamma-C.	26
Figure 25: Detail of Figure 24. The non-periodic short Sub Diurnal Radon (SDR) signals are very similar in the record of the lateral gamma detectors, but do not appear in the record of gamma-C.....	27
Figure 26: Detail of SDR signals recorded by the external gamma sensors. The high concordance of these signals indicate that the source is located in a position which is symmetrical to both sensors. In one case a related response possibly occurred at alpha-H.	27

Figure 27: A 10-day interval of the record of the measured signal from the two external gamma sensors flanking the tank, compared with the synchronous record from the internal gamma-C. The two external sensors show a DR signal that is approximately in phase, and in anti-phase with gamma-C. A semidiurnal component is apparent in all three cases. 1-Hour resolution. See text.....	28
Figure 28: Spectra of the records of an external gamma sensor (gamma-W) and the internal gamma sensor (gamma-C), during 350 days (measured signal; 1-hour resolution). Periodicities S1 and S2 are clearly observed also at the external sensor, but with different relative amplitudes.	29
Figure 29: The temporal variation of amplitude and phase of the diurnal periodic variation measured by sensor gamma-W. See text.	30
Figure 30: A 10-day interval of the record from gamma-E sensor with a 5 cm thick Pb shield in front, blocking the direct radiation from the air volume of the tank. 1-Hour resolution. See text.	31
Figure 31: Topview of experimental setup during CI-5, using 10x10x5cm Pb bricks to shield gamma-E from radiation originating from the northern half of the tank (detector gamma-W is not shown).....	31
Figure 32: Time series of the Daily Mean (DM) of the lateral gamma sensors and gamma-C during CI-5 interval, with the partial blocking of gamma radiation to gamma-E. The overall level of radiation at gamma-E is reduced. See Text.....	32
Figure 33: Detail of Figure 32 exhibiting the apparent seasonal pattern in the DM time series of the lateral gamma sensors, compared to the internal gamma-C. The vertical scale of the lateral sensors is 50% of the scale for gamma-C. Multi-Day (MD) variations are superimposed on the seasonal variation. See text.	33
Figure 34: Time series of the Daily Amplitude (DA) of the lateral gamma sensors and gamma-C during CI-5 interval, with the partial blocking of gamma radiation to gamma-E. See text.	34
Figure 35: Correlation diagram of the Daily Amplitude (DA) among the lateral gamma sensors during CI-5 interval, with the partial blocking of gamma radiation to gamma-E...	35
Figure 36: Multi-Day (MD) variation patterns during CI-5 interval.	36
Figure 37: A 20-day long time series of the measured signal of the lateral gamma sensors during CI-5 interval, with the partial blocking of gamma radiation to gamma-E. The net scale for both sensors is 10 Kcounts. The MD signals reflected in both sensors are concordant and with very similar intensity. The DR signals are reduced to around 50% in gamma-E. See Text.....	37
Figure 38: Detail of the DR signal (after decomposition) at the external gamma detectors. Note the reduced signal (~50%) at gamma-E. See text.	37

List of Tables

Table 1: Technical data of experimental setup	5
Table 2: Chemical composition of phosphorite	5
Table 3: Complementary investigations (CI) around the experimental tank	22
Table 4: Statistics of daily variation at the two external and the internal gamma detectors ..	32

Abstract

Temporal variation phenomena and signals of Radon (Rn-222) are simulated in a +1 year long passive experiment within closed confines. The setup consists of a sealed 0.64 m³ metal tank filled with 0.4m of ground phosphorite (376 kg; 175 ppm U) serving as the Rn source. Rn in the overlying air volume (384 liters) is released from the natural rock and is maintained in contact with it. Vertical internal sensors consist of gamma-C (within a lead pipe) and two alpha detectors at two levels – alpha-H and alpha-L. Gamma-C detects gamma rays originating from Rn in the air volume and from the upper 0.2 m of the phosphate (U, K, and Th - stable). Alpha-H and alpha-L detect alpha particles from Rn in their ~50 cc sampling cup. Two external lateral gamma sensors (gamma-W and gamma-E) are placed at the level of the air volume of the tank.

Following attainment of a secular equilibrium level non uniform variations of the radiation are recorded by the internal sensors and at the external sensors. The fluctuations are up to around 20% of the equilibrium level (alpha radiation). Periodic and non-periodic signals occur, of different time scale: a) Periodic seasonal radon (SR) signals; b) non-periodic multi day (MD) signals; c) periodic daily radon (DR) signals, and non-periodic sub-diurnal radon (SDR) signals. Similar, related, inversely-related and dissimilar temporal patterns are manifested in the time series recorded by the sensors.

Periodic diurnal components indicative for gravity tide are absent in the DR signal. The DR signal is dominated by the solar tide components S1, S2 and S3 (24-, 12-, 8-hour periods). Unlike relative amplitudes and different phase of these components occur among the sensors. SR signals are manifested in the measured signal (MS) and in the temporal pattern of the net daily amplitude (DA). A compound association among the periodic signals occurs in the SR variation of the amplitudes and phase of the solar periodicities of the DR signal. These characteristics link the periodic phenomena to the rotation of Earth around its axis and its rotation around the sun.

Non-periodic MD signals show both related and unrelated patterns among the internal alpha and gamma sensors. The lateral external sensors show conforming DSR signals and MD signals, which are different from the pattern of MD at the internal sensors. These characteristics indicate a varying radiation field which differs in the outside-inside dimension of the system, and is symmetric in the external east-west direction.

The different manifestations of the signals at the various sensors indicate that: a) the varying radiation originates from radon and its immediate daughters in the gas phase, mainly in the air of the upper volume of the tank, and also from air in the pores of the phosphorite; b) the radiation is spatially inhomogeneous within the tank, and c) dissimilar temporal gamma radiation patterns pervade inside and outside the tank.

The variations cannot be accounted for by a temporally varying non-uniform Rn concentration within the tank. Exchange of radon between the tank and the external environment and atmospheric-environmental influences are negated based on the physical configuration of the experiment and on atmospheric measurements. Lacking other internal processes and considering the credence of the external solar influence on the signals it is assumed the non-periodic variations are also due to external influences.

At face value the results indicate that unrecognized processes are involved in the generation of the radiation patterns. It is suggested that a remote varying influence of an irradiative nature interacts with mineral lattices of the phosphorite to form a secondary local field, the latter being related to the geometry of elements of the experiment. This non-homogenous and secondary field drives in turn the radiation pattern from the uniform and stable concentration of radon in the gas phase. The interim suggestion is that this leads to a spatially non-homogenous nuclear radiation emitted by the system, which is also varying in time as a function of the primary external driver.

These conclusions are similar to conclusions arrived at from observations in the geological environment. The temporal variations of the MS signal and its characteristics of the experiment resemble signal types (SR, MD, DR, and SDR) and properties encountered at subsurface sites.

Introduction

Radon (^{222}Rn) is a radioactive inert gas formed by disintegration from ^{226}Ra as part of the ^{238}U decay series. It occurs at varying concentrations in geological environments. The combination of its noble gas character and its radioactive decay makes it a unique ultra-trace component for tracking temporally varying natural processes in subsurface systems. The application of stress to rocks is thought to enhance the emanation of radon from the solid phase, rendering radon a potential sensitive tracer of geodynamic processes in the upper crust.

The proposition that radon may serve as a useful proxy for seismic activity has been repeatedly considered (e.g. Monin and Seidel, 1992; Segovia et al., 1995; Toutain and Baubron, 1999; Hartmann and Levi, 2005 and references therein). In parallel, transport of radon in soil and water has been investigated as a tool for monitoring volcanic activity (e.g. Cigolini et al., 2001; Burton et al., 2004; Alparone et al., 2005; Immè et al., 2006). Radon is used in these scenarios as a highly sensitive tracer of secondary geodynamic processes – mainly mechanical and thermal. Using nuclear techniques the measurement sensitivity for radon in the subsurface geogas is extremely high and can be performed with a time resolution in the order of 1 hour or less. Despite the presumed advantages of radon as a geophysical proxy, the utilization of radon in geodynamics has been hampered by the complex patterns of the measured signals. Radon time series display a compound temporal pattern of variation spanning multi-years to several hours, and exhibit both periodic and non-periodic patterns.

Few recent works describe results of high resolution Rn monitoring in the unsaturated zone. Trique et al. (1999), using measurements in a tunnel within massive gneiss, associated multi-day Rn bursts with transient deformation due to loading and unloading of a local water reservoir. Reddy et al. (2004) and Steinitz et al. (2005) describe a rare type of multi-day Rn signal with a Rn-decay decreasing limb. Using an 8-year record of Rn, obtained next to a major active boundary fault of the Dead Sea Rift (DSR), a statistically significant relation between multi-day Rn signals and earthquakes in the nearby sector of the DSR was demonstrated by Steinitz et al. (2003). In these works the establishment of the geodynamic nature of the signatures and signals is based on negation of atmospheric influence, analyzing radon signatures in the geological, spatial, time and frequency domains and, primarily, on correlating radon with geophysical phenomena, and specifically the correlation to earthquakes (Steinitz et al., 2003; Begin and Steinitz, 2005).

Intensive high-time resolution (<1 hour) monitoring of Rn is being performed since 1995 in upper crustal rock systems, along the western margin to the Dead Sea transform (DST), in the frame of the Israel Geodynamic Radon Project (IGRnP). Presently radon is being monitored in a 200 km segment along the western boundary fault of the DST, from the Dead Sea to the Gulf of Elat (Aqaba). The Rn signals are characterized by: a) clear-cut temporal variation types; b) recurrence at the different locations within the same geologic unit; c) similar features recorded in diverse geographic, geological and geodynamic situations. The main types recognized are multi-year, seasonal radon (SR; periodic), multi-day (MD), diurnal radon (DR; periodic) signals (Steinitz et al., 1992; Steinitz et al., 1996; Steinitz et al., 1999) as well as intense variations lasting up to several hours (Balogh and Steinitz, 2004). These signals are assumed to be due to natural processes as they recur systematically in time and at different stations.

An important advance in the geophysical understanding of these radon phenomena was recently demonstrated by analyzing a unique data set from the subsurface of a single granite pluton at the scale of 1km, serving as a type locality for the phenomena (Steinitz et al., 2006; Steinitz et al., 2007, Barbosa et al., 2007). A new geophysical framework for the temporal patterns of radon was obtained by: i) applying advanced time series methods and signal processing approaches in the time and frequency domain to long (multi-year) and high-resolution (< 1 hour) radon time series for the extraction and description of the superimposed signals; ii) the analysis of the environmental and geophysical influences on radon time series; and iii) both multi-site and multi-parameter analysis of radon phenomena and other geophysical phenomena. The primary outcomes concerning the radon signal in the subsurface are: a) the compound variation is composed of a periodic seasonal radon (SR) signal, diurnal (24-hour) and semi-diurnal (12-hour) radon (DR) signals and non-periodic Multi-Day (MD) signals; b) the MD signal may represent transients of a mechanical affiliation; c) the SR and especially the DR signal are probably generated in the subsurface by a solar irradiance related process.

The understanding of the origin of the different radon signals and its geophysical interpretation is a challenging task. A primary assumption is that the temporal patterns cannot be generated in the geogas phase since the source of the radon is in the country rock and the processes releasing and driving it by emanation into the geogas environment act on the rock system. Different explanations have been raised for the origin of the periodic signals observed in radon time series, including the influence of environmental factors, mainly atmospheric pressure (Shapiro et al., 1985; Ball et al, 1991; Pinault and Baubron, 1997; Finkelstein et al, 2006) and tidal mechanisms (Aumento, 2002; Weinlich et al, 2006).

This contribution seeks to advance the understanding of the temporal variation phenomena of radon in the geogas system by mimicking and investigating the signals formed in a laboratory experimental setup at confined conditions. The different signals encountered are investigated with the periodic diurnal signals serving as a key object.

Experiment Phases and Stages

The set of different experiments performed with the setup was carried out in two major phases.

- a) The original goal of the system, performed inside a laboratory of Soreq Nuclear Research Center (SNRC; Yavne) was for conducting short calibration experiments, lasting up to several tens of days, of electronic alpha and gamma detectors, summarized by Vulkan et al. (1998). These calibration experiments, in the years 1996-1998, led also to the inadvertent observations dealt herein. The initial observations led to further short investigations in SNRC (1999-2003). Results from this phase pertaining to environmental influences are referred to and utilized in this Report.

- b) The experimental facility was transferred to the Geological Survey of Israel (GSI, Jerusalem) and was set up under an open shack, in the original configuration while utilizing a new set of sensors of the same types. A long term experiment was initiated in the beginning of 2007.

This contribution refers to the primary experiment as conducted in the second phase, and describes also complementary observations from initial experiments conducted in the first phase.

Experimental Setup

The experiment is performed in a square tank constructed of welded 3mm thick iron plates (Fig.1, 2; Table 1). The topside is fitted with three metal boards (planks) bolted into square profiles at the topside. Three metal tubes, suspended vertically into the volume of the tank from the central board, serve for the insertion of radiometric sensors. Additional (1.5") inlets in the external top cover boards serve as feed-through for additional sensors. The internal volume of the tank is sealed from the environment with gaskets in the tubes and plate rims. Sealing of the cover plates is further secured with silicon glue.

The upper sub volume of the tank contains air and the lower part of the tank is filled with ground phosphorite, obtained from the Oron mine in the north-western Negev. The uranium (radium-226) in this material serves as the source of radon in the air of the experiment.

The technical characteristic of the experimental setup are given in Table 1, and the chemical composition of the phosphorite in Table 2.

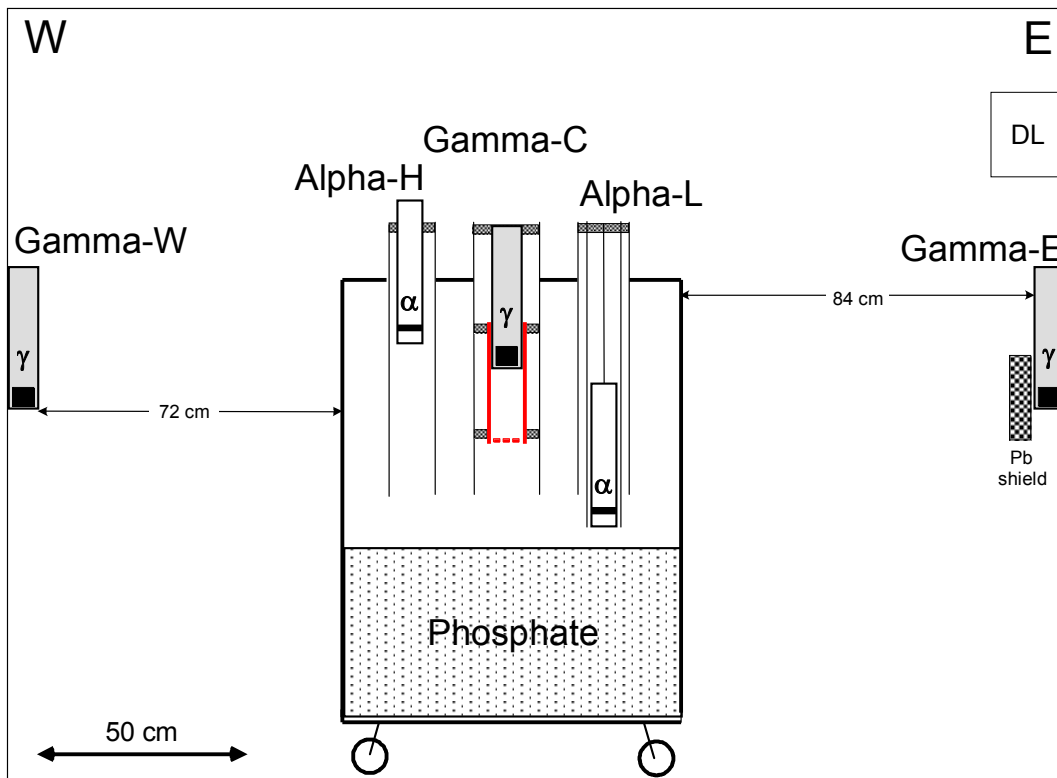


Figure 1: Experimental layout showing the tank with the phosphorite, the internal gamma and alpha sensors and the position of the two external lateral gamma sensors. Gamma-C is immersed within a lead tube (0.5 cm thick). The radiation shield in front of gamma-E is also indicated. DL – data logger.

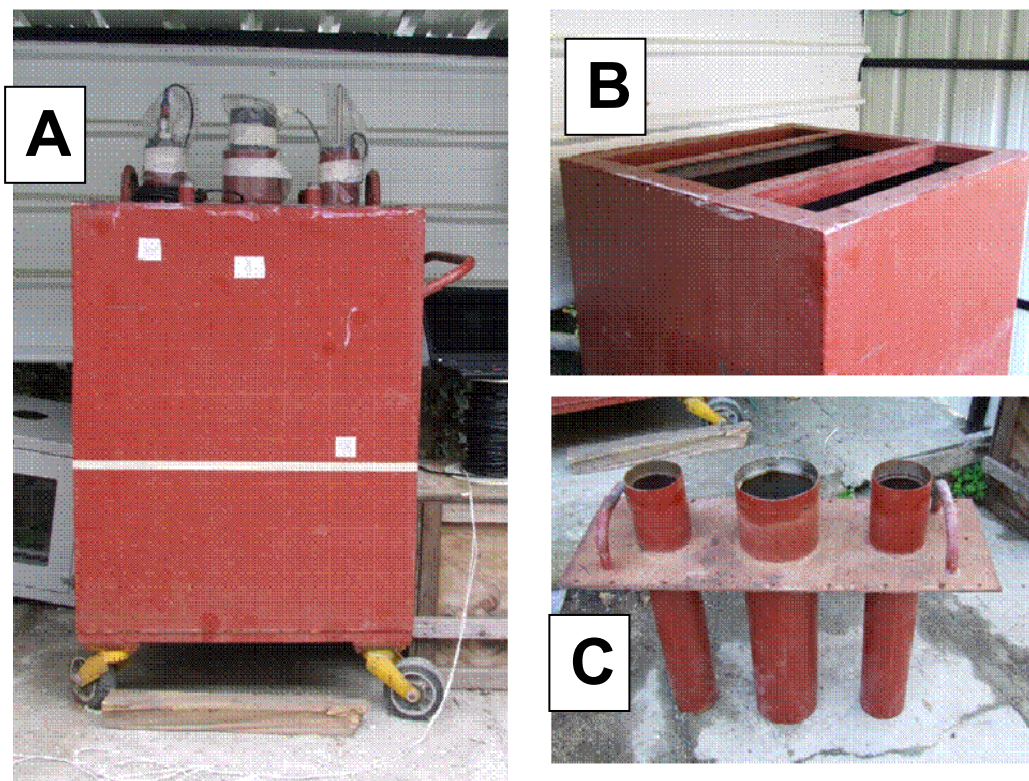


Figure 2: The experimental setup. A – Front view of tank with indication (horizontal mark) of internal phosphorite level. Three radiation sensors are inserted from the top; B – tank with upper planks removed; C – central plank with tubes for inserting sensors. Sensors are inserted with gaskets.

Table 1: Technical data of experimental setup

	Description / unit	Quantity	Remarks
Dimensions	Width (cm)	80	
	Depth (cm)	80	
	Height (cm)	100	
Phosphorite in tank	Height (cm)	40	
	Weight (kg)	376	
	Volume (liter)	256	
Mineralogy	Francolite	>95%	XRD
	Calcite	~1%	
Uranium	Concentration (ppm)	175	
Radon-222	Background activity in tank open to the air (kBq/ m ³)	< 0.35	Based on measurements in phase I using alpha detectors
	Total activity in air of tank (kBq)	97.4	
	Specific activity in air of tank (kBq/m ³)	254	

Table 2: Chemical composition of phosphorite

	%	%	%	ppm
SiO ₂	1	MgO 0.3	SO ₃ 2.26	Sr 1700
Al ₂ O ₃	0.12	Na ₂ O 1.28	Fe ₂ O ₃ 3.82	Ba 772
Fe ₂ O ₃	0.26	K₂O 0.05	LOI 7.74	Th 0.784
TiO ₂	0.05	P ₂ O ₅ 33.18	F corr 1.61	U 175.4
CaO	52.24			

Radiation Detectors

Different radioactive alpha and gamma sensors were used in the calibration experiments conducted during the first phase (p. 9). A new set of similar radiation detectors were used in the second phase – placed within the tank and outside. Environmental sensors were utilized during one experiment of phase 1 (inside and outside the tank) and during phase 2.

Two types of radiation detectors are utilized in phase 2:

- a) Gamma detector – A 2"×2" NaI detector (PM-11 detector, ROTEM Inc., Israel), recording gamma-ray impulses of energy above 50keV. Utilization of gamma detector systems for monitoring Rn is based on the detection of gamma radiation from the ²¹⁴Bi, and to a lesser extent those from the ²¹⁴Pb (Steinitz et al., 2005). Due to the short half lives of the Rn daughters, equilibrium of the Rn and its daughters is achieved after a short time (~25 minutes).
- b) Alpha detector - Barasol BT45N detector (450 mm² Si diode; Algade Inc., France). The detector is equipped with a cellulose filter. Alpha radiation impulses originating from ²²²Rn are recorded (as counts). The producer given sensitivity of Alpha-H is 42.6 Bq/m³ per 1 count/hour and 51.9 Bq/m³ per 1 count/hour for Alpha-L.

Three radiation detectors are inserted into the tank via the vertical tubes on the top, separated from the external atmosphere by gaskets. A gamma sensor (gamma-C) is inserted into the tank into the central tube enclosed (immersed in the upper third) within a lead pipe (length 30 cm, O.D. 10.5 cm and thickness of 0.5 cm). A round plate with holes is placed horizontally at the lower end of the Pb pipe. The lead shield serves to reduce the background radiation emitted from the phosphorite below while allowing gas exchange between the measurement cell and the air volume of the tank. Two alpha detectors are inserted into the two further vertical tubes, flanking the gamma-C sensor. The eastern detector is placed around 47 cm above the phosphorite (alpha-H) and the western one approximately 5 cm above the phosphorite.

Two additional gamma sensors are added outside the tank in lateral and vertical positions to the east and west of the tank, approximately centered opposite the air volume of the tank (Fig. 1).

Data Collection and Pre-Processing

Data collection was implemented with a data logger (Campbell Inc.) at a sampling rate of 15-minutes. Time is shown on a decimal-day scale (Day 0 = 1.1.1992; UT), as utilized by the IGRnP. The timing precision is better than ± 10 seconds. In phase-II the tank was closed on Day 5503.5 (25/01/07), and electronic measurements commenced on Day 5507.7 (29.01.2007).

In general it is accepted that in a closed environment radon build-up levels off after 3 weeks, once secular equilibrium between Ra-226 and Rn-222 is obtained. Thus secular equilibrium is assumed from Day 5525 onwards.

The measured time series are pre-processed by:

1. Decimation to files of hourly and daily averages
2. Decomposing the time series using a 25-hour sliding average to separate the multi-day and the diurnal variation
3. Calculation of daily amplitude (DA) between daily extremes

Additional Measurements and Complementary Investigations

Ambient temperature and pressure are measured during both experimental phases. Concurrent pressure and temperature inside the tank, performed in phase-I, are used below.

The pattern of the external gamma radiation due to radon inside the experiment tank is examined by using an external radiation source and additional detectors.

Results

Signal Patterns

Background measurements with alpha and gamma detectors with the tank open to the atmosphere (aerated) were performed during phase I and are summarized by Vulkan et al (1998). In terms of alpha measurement the background in the tank is less than 0.35 kBq/m^3 . The count rate of the internal gamma-C detector is affected by radiation from four sources: a) radon (Rn-222 as Bi-214) in the air of the tank; b) radiation originating from radioactive elements (U, Th, K) in the phosphorite; c) external environmental gamma radiation, and d) radiation, originating from Rn in the interstitial air of the upper 20 cm of the phosphorite. The volume of the latter interstitial air is estimated to be 5-10% of the upper volume. Ignoring the relatively low external component the background radiation recorded by a PM-11 gamma sensor is in the order of 85 Kcounts/15-minutes.

As expected, once the tank is closed build-up of radon is observed inside. The concentration of radon in the air volume increases due to its emanation from the phosphorite and at the same time radon also decreases due to radioactive decay (half-life = 3.82 days). The outcome of these two processes is that secular equilibrium, observed as a plateau level, is attained after some 20 days by the three internal sensors, around Day 5525 (Figure 3). The two alpha detectors show the same level, a level which is also in accordance with those reported by Vulkan et al. (1998). Using the daily averages a linear correlation is observed among the alpha detectors (Figure 4).

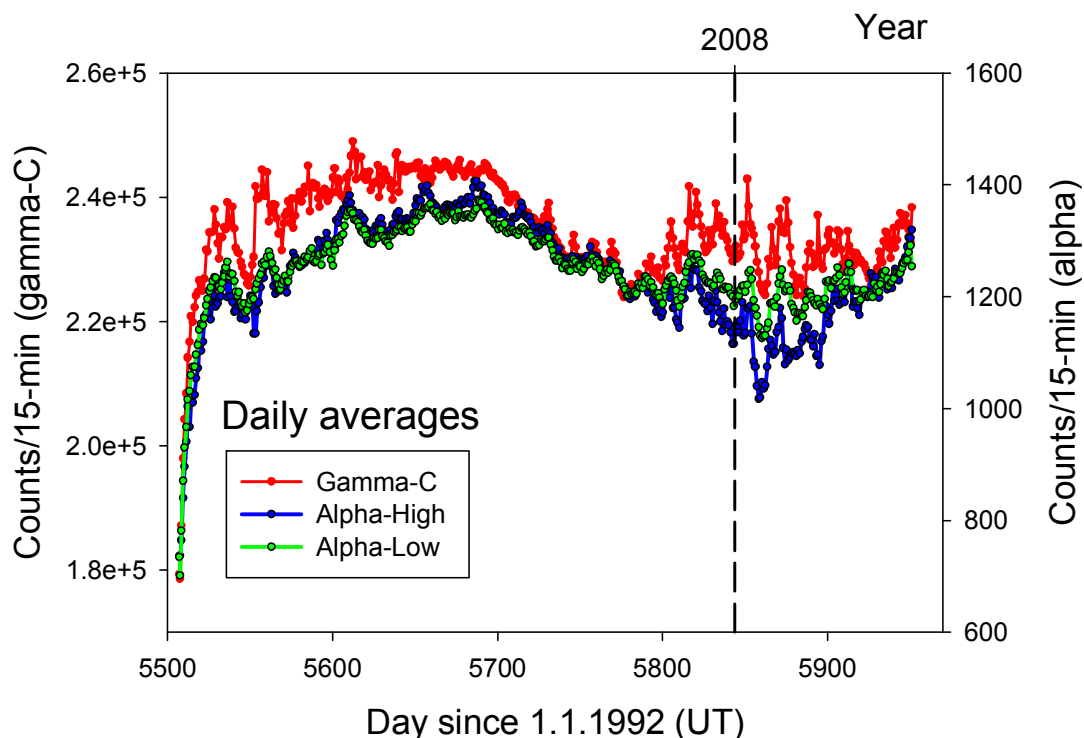


Figure 3: The daily average radiation registered by the internal radiation detectors

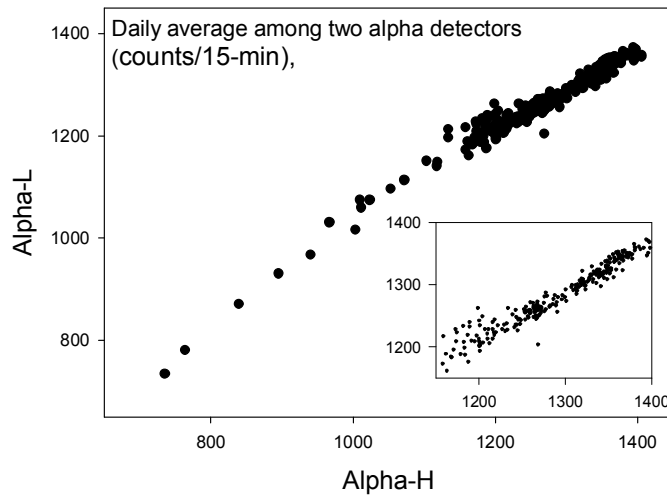


Figure 4: Correlations of daily average among the alpha detectors, during and following the initial build-up of radon in the tank

In the interval following the build-up, in difference with the expected pattern, variations are observed in the level of radon, in both alpha and gamma radiation detectors. In terms of the alpha detectors these variation are in the range of up to 20% of the overall level. Different types of variation are encountered. The signals are classified based on the temporal scale of the variation, applying the nomenclature used for signals occurring in the natural subsurface environment (Steinitz et al., 2007). The types of variation observed are:

- Seasonal variation of radon (SR), probably periodic at 1 cycle/yr
- Multi-Day (MD) signals, lasting 2-20 days, which are non-periodic
- Diurnal Radon (DR) signals, which have typical periods of 24-, 12- 8-hours (S1, S2, S3)
- Sub-Daily Radon (SDR) signals, occurring sporadically and lasting several hours. These signals are observed by the external detectors and will therefore be dealt later.

The long term variation pattern of the radon level at secular equilibrium in the tank is shown in Figure 5 using daily averages. A clear seasonal (SR) variation is indicated by the three internal sensors, with high values in the summer and low levels in winter.

Additional irregular fluctuations Multi-Day (MD) signals are encountered on the SR signal in Figure 5. The fluctuations are jointly observed by the two alpha detectors and in part also by the gamma-C detector. The fact that these fluctuations last for several days and that they are concordant at the two alpha detectors implies that they are not due to instrumental artifacts.

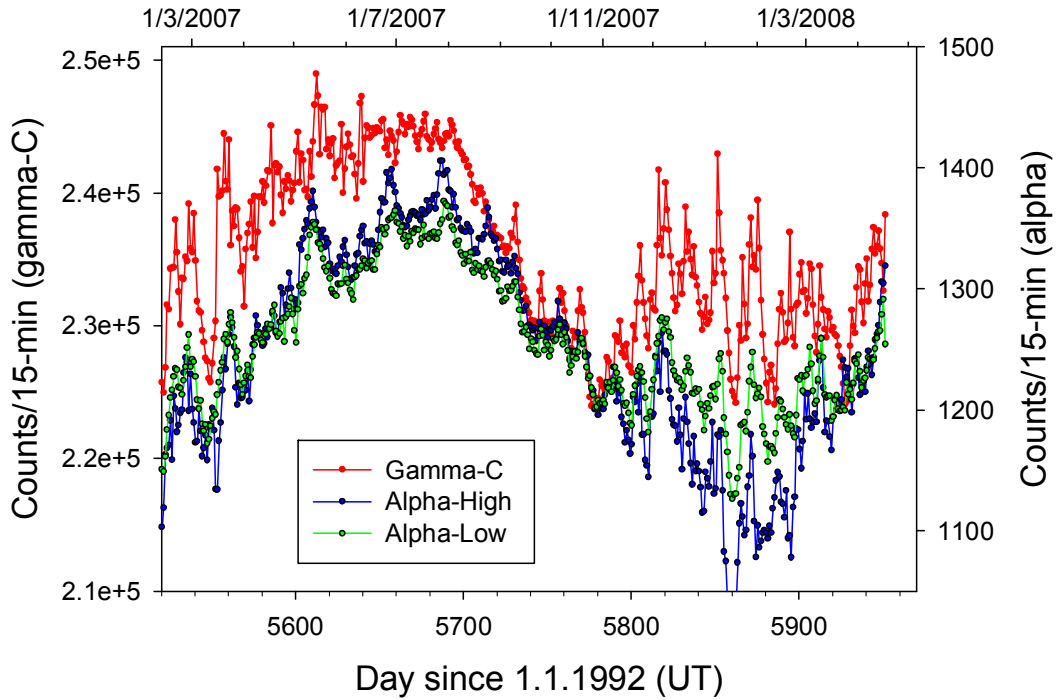


Figure 5: Time series of the daily average in the plateau interval (following initial build-up from Day 5503 to 5525) as recorded by the three internal radiation detectors

The short term MD and DR variations, superimposed on the SR signal within the tank are demonstrated and emphasized by decomposing the measured signal using a 25-hour sliding average, as implemented by Steinitz et al., (2007). This type of decomposition highlights the irregular non-periodic multi-day (MD) variation lasting 4-20 days, and the periodic Daily Radon (DR) signal.

The non-periodic MD signals are registered by all three internal sensors, but in varying forms (Figure 6). During different intervals the three sensors display both concordant and discordant patterns for this type of signal (Figs. 7-8). The two alpha detectors record the same MD signals, having similar forms and amplitudes. In parts of the time a temporal offset of the MD signal is observed among the two alpha detectors – with a lag of up to several days (alpha-L lagging?; Figure 8). A different pattern of the MD component is shown by the gamma-C signal, relative to the MD variation of the alpha detectors.

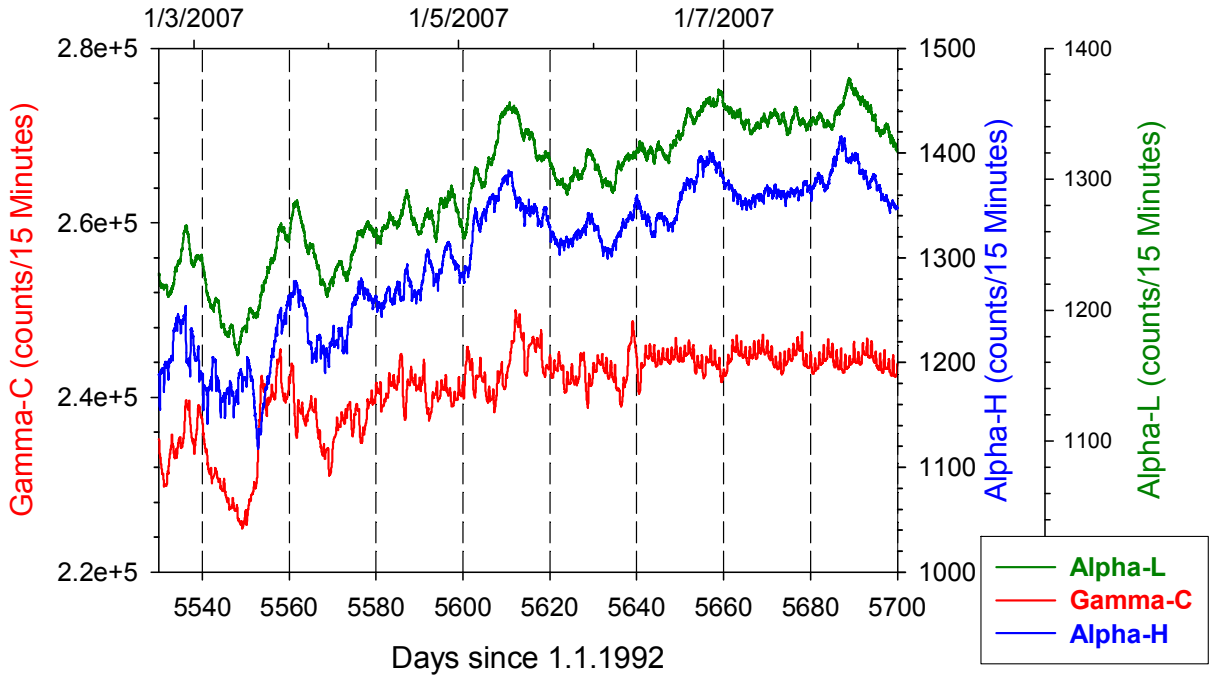


Figure 6: A 170-day long segment of the smoothed time series of the internal radiation detectors showing a multi-day (MD) variation. Different co-variation patterns are observed among the sensors. See text.

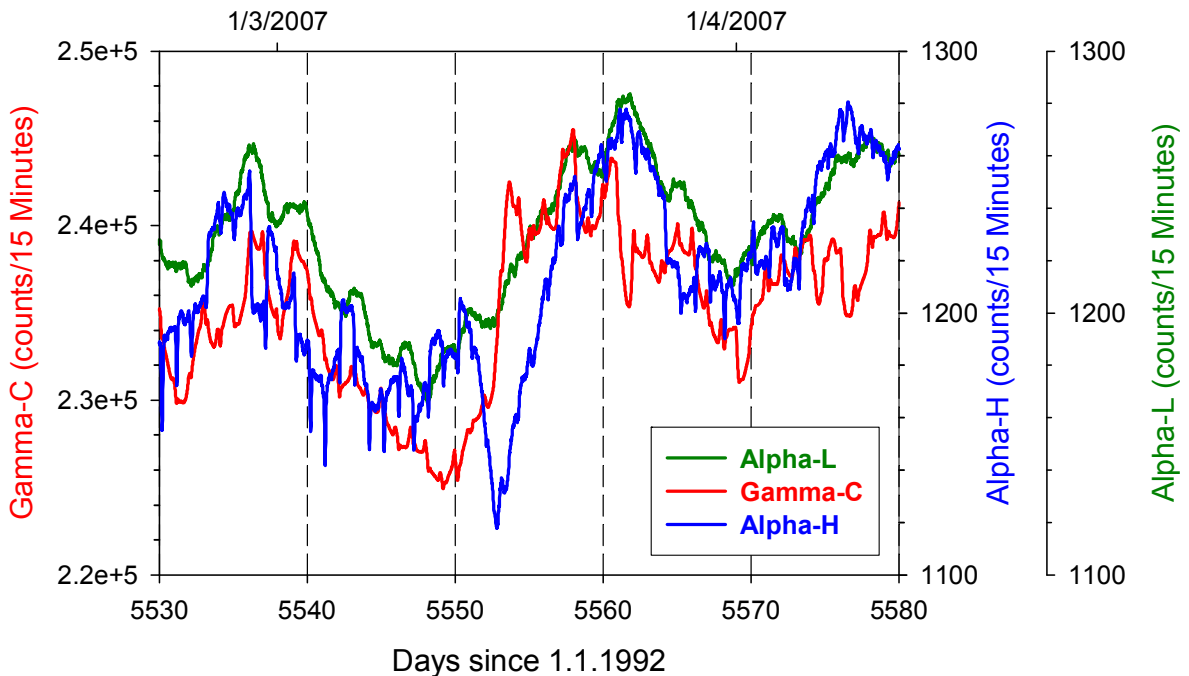


Figure 7: Detail of Figure 6 showing corresponding MD patterns among all three sensors. See text.

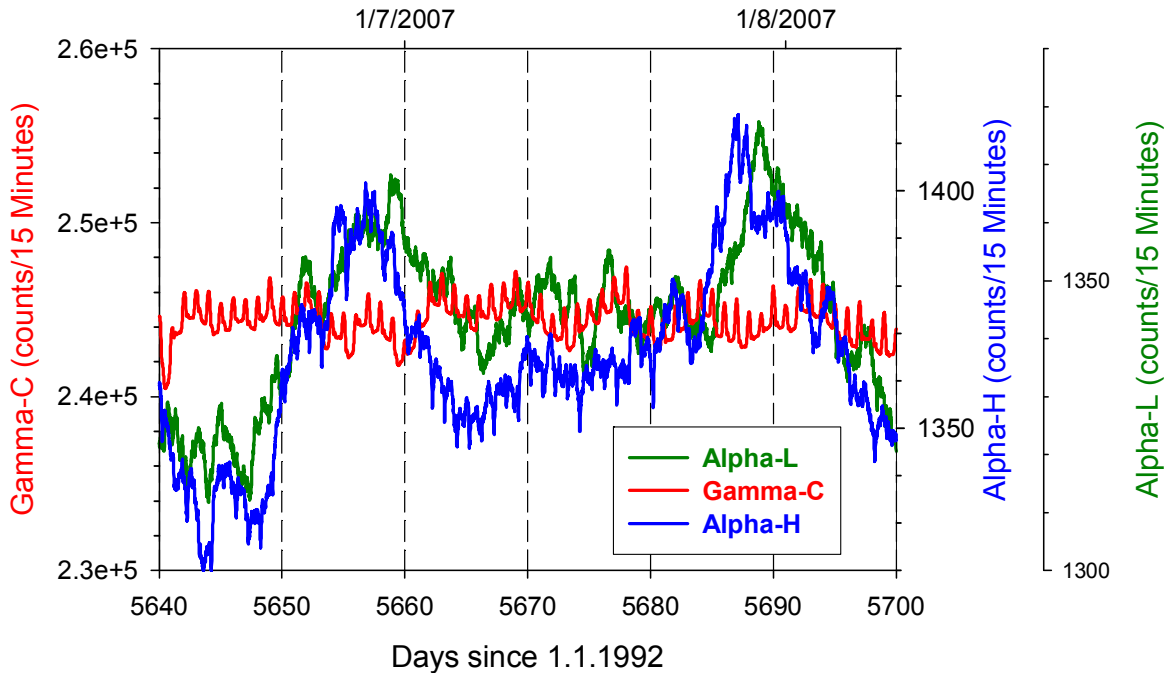


Figure 8: Detail of Figure 6 showing matching MD patterns among the two alpha detectors and a dissimilar variation pattern of the gamma-C. Time lags of up to few days of the MD signal occur between the alpha detectors. See text.

Diurnal Radon (DR) signals, dominating the overall variation, are clearly observable in the time series as large daily variations of gamma-C and alpha-H sensors, in the order of 10% of the measured signal (Figure 9). In the case of the gamma-C detector the proportion is actually much larger, due to the fact that this signal contains a fixed contribution from the direct radiation from the phosphorite ("background" of 85.84 Kcount/15-minutes; Vulkan et al., 1998). Alpha-L shows a much smaller DR signal, compared to the large signals encountered by alpha-H and gamma-C. A relation between the DR and MD patterns is not observed.

Different forms of the DR signal are observed (Figure 10, 11). The DR signal of gamma-C signal has a sharp peaked form rising above the secular equilibrium level. In contrast, the alpha-H signal shows sharp peaks that protrude downward, below the equilibrium level, indicating an apparent fast deficit in radon. Comparison among the sensors indicates that relative offsets in time exist, indicating a different phase the DR signal among the different detectors. Spectral analysis of these time series shows that the daily signal is composed of a major 24-hour and a minor 12-hour cycle (see below).

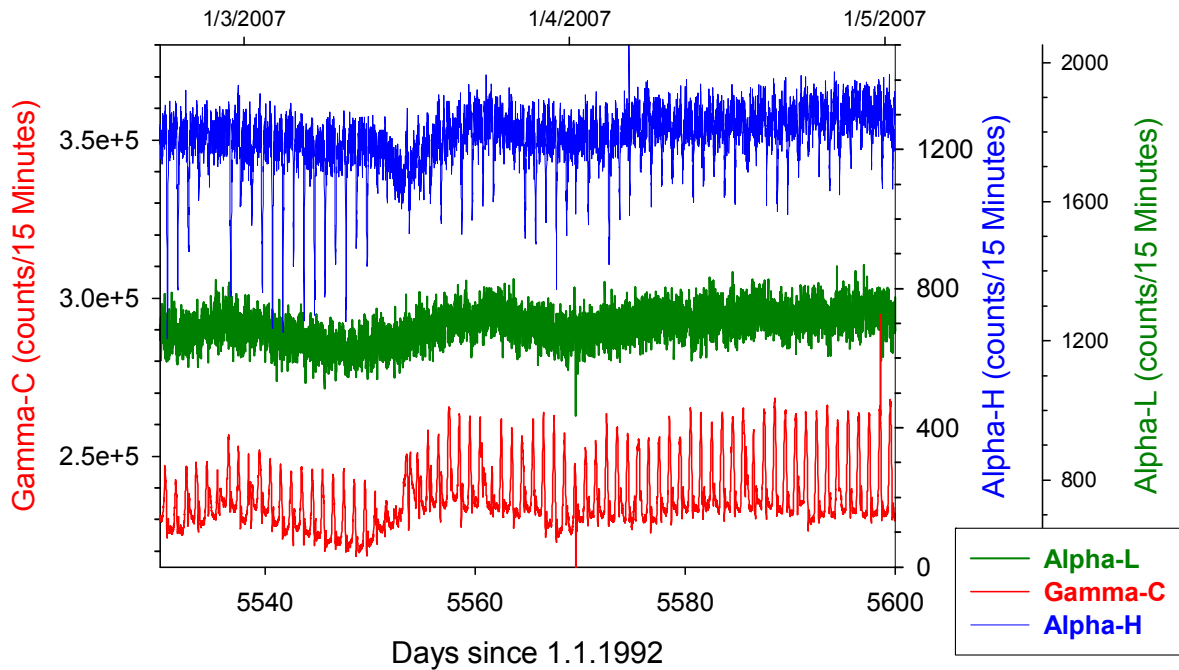


Figure 9: A 70-day long segment of the measured signal recorded by the internal radiation sensors showing the multi-day (MD) and diurnal radon (DR) variation. MD signals are recorded by the three sensors and DR signals, having different appearance, are dominating the time series of alpha-H and gamma-C.

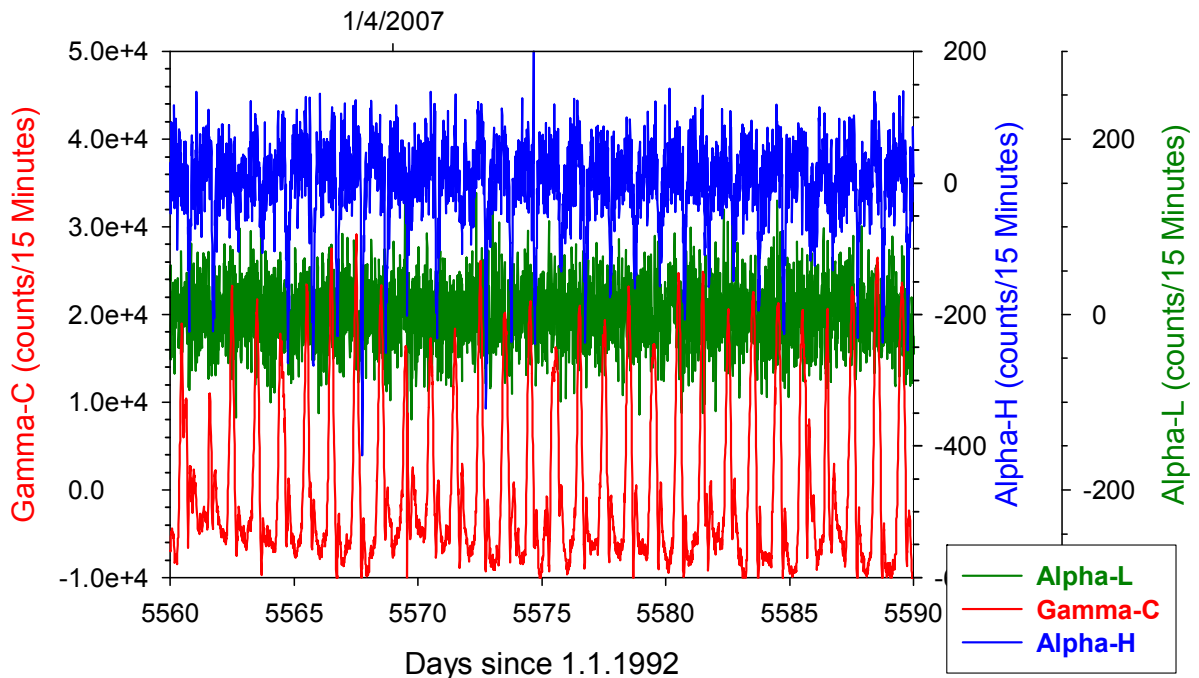


Figure 10: The daily variation of the radiometric signal in the tank, extracted as the residual of the 25-hour smoothing. Different relative scales and different DR patterns characterize the signal of each sensor. See text.

The observations on the temporal pattern of the SR, MD and DR signals recorded by the internal sensors are summarized as follows:

- The three internal sensors exhibit overall similar behavior of the measured radon signal, in accordance with the expected build-up and maintaining of a secular equilibrium pattern for radon within a confined enclosure;
- Notwithstanding diverse secondary variations are superimposed on the secular equilibrium level, consisting of signals of different time scales;
- The sensors exhibit dissimilar patterns of these secondary signals;
- All three internal sensors exhibit a clear long term seasonal radon (SR) signal. This is recorded using two different measurements systems: two alpha detectors and one gamma detector; The pattern of this SR signal differs among the two sensors that illustrate it;
- Multi-day (MD) signals are recorded by all sensors, with concordance that varies in time;
- Daily radon (DR) signals are manifested among the sensors with different amplitude, form and phase;

The three sensors are immersed in a gas system with a basically uniform distribution of radon. The overall related but dissimilar patterns among the sensors, especially of the daily variation, cannot be attributed to different concentrations of radon within the closed volume. The immediate implication is that such variation patterns cannot be explained in terms of a varying concentration of a component (radon) of the gas phase within the confined system.

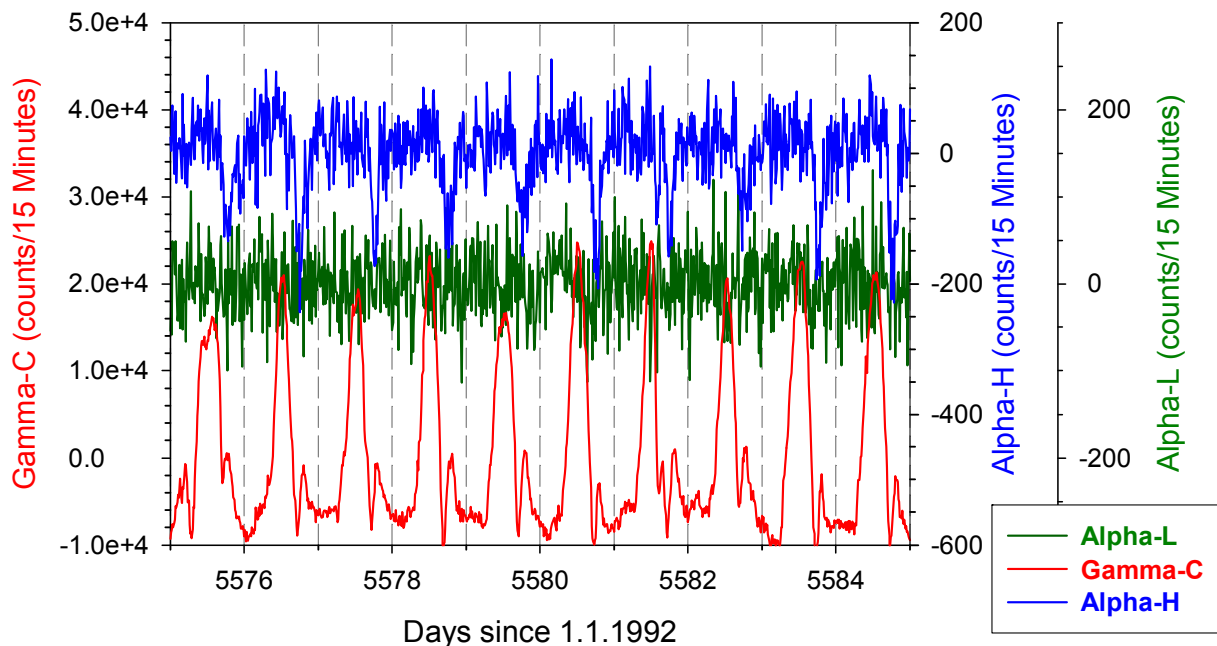


Figure 11: 10-day detail of Figure 10 showing the DR signals recorded by the internal radiometric sensors. A DR signal is barely observable at alpha-L. Large but highly differing DR signals, primarily in phase, are recorded by alpha-H and gamma-C. The daily cycle dominates, but a semi-diurnal component is clearly observable in the gamma-C signal. The relatively low S/N signal of the alpha detectors does not enable distinguishing a semi-diurnal component in them.

Environmental Influences

Pressure and temperature variations are often invoked as possible drivers of variations of the radon signal in shallow geological environs. Based on many observations at shallow levels (primarily in soil) this approach relies on the similarity of temporal patterns in the time series (at seasonal to daily scale) and on the fact that one is dealing with a component in a gas system, often in connection with atmospheric air.

The relation of barometric pressure and ambient temperature with the radon signal observed in the tank were specifically investigated in experiments already performed during phase-I. To this end temperature and pressure sensors were installed inside the tank.

It can be assumed that the tank wall, made of iron plates, is in thermal equilibrium with the surrounding ambient temperature. Comparing pressure measurements inside and outside the tank shows that the internal pressure is also in equilibrium with the atmospheric pressure (Figure 12). This equilibrium is probably attained by slight flexing of its thin walls and via minor leaks along the seams.

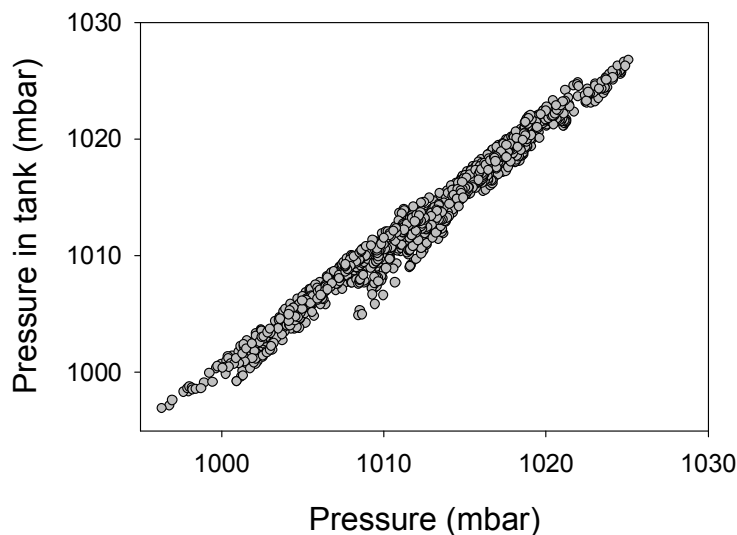


Figure 12: Dependence of pressure inside the tank on the external ambient air pressure. Hourly averages in Days 3680-3739.

Simultaneous measurements of pressure, temperature and radon (as gamma radiation at gamma-C) indicate that both these environmental parameters cannot be considered as the direct drivers of the variation attributed to radon (Figure 13). The intricate semi-linear patterns observed in different parts of the diagrams are related to the fact that the wavelengths of temperature and pressure variations are comparable with those of the radon time series.

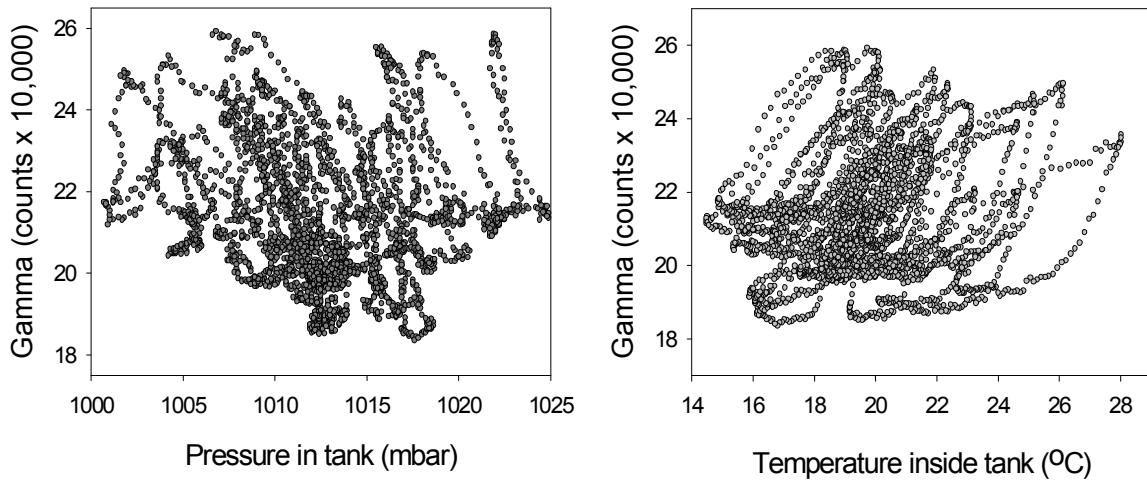


Figure 13: Relation between hourly averages of the radiation level at gamma-C sensor and pressure (left), and temperature (right).

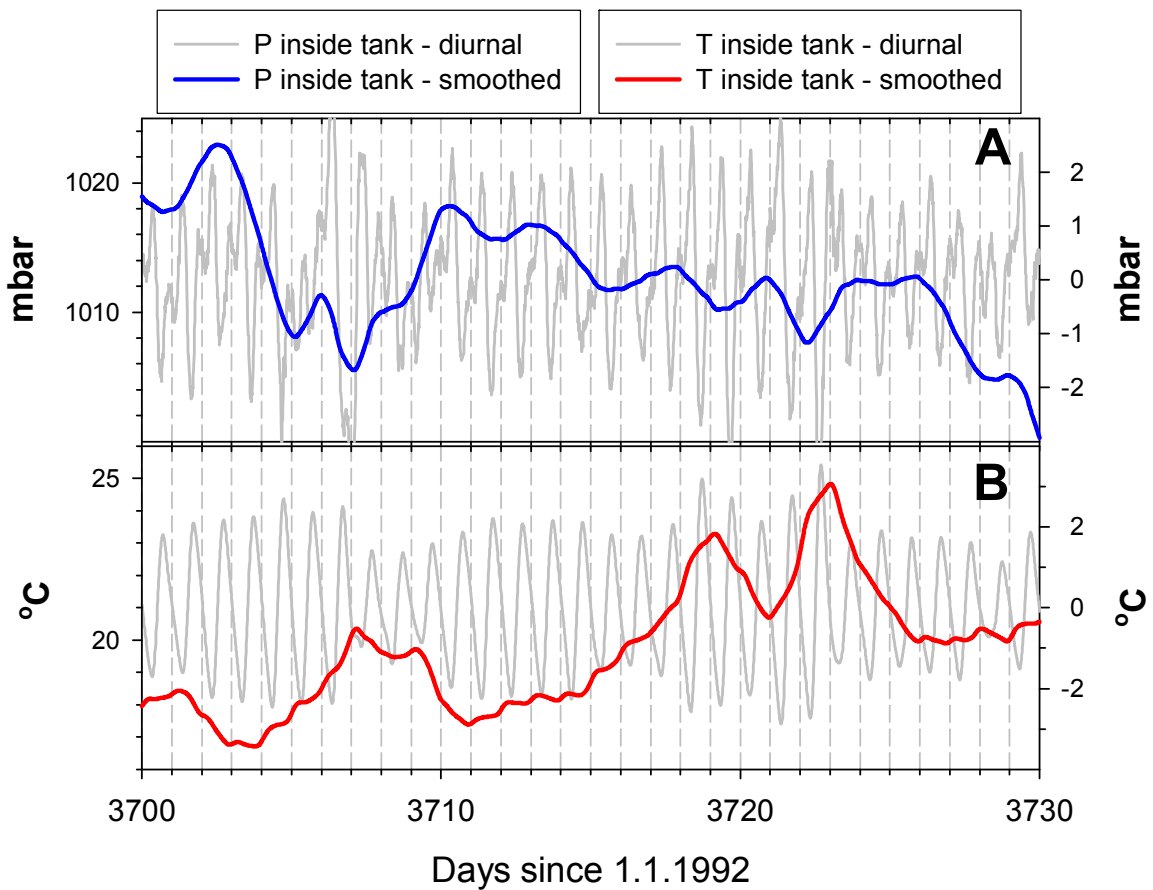


Figure 14: Pressure (A) and temperature (B) variation inside the tank. Each time series is shown decomposed (using a 25-hour sliding average) to the periodic daily variation and the longer term variation. The longer term variations are used in Figure 15.

The temporal variation of atmospheric temperature and pressure contains diurnal periodic components and longer term non-periodic variations. In this respect a resemblance exists with the variation patterns of radon in the tank. The comparison of the diurnal variation of temperature and pressure with the diurnal variation of radon is somewhat complex due to the correspondence of their periodicities. Therefore the issue is further investigated using the longer term variation.

Using a 30-day long interval (from phase-I) the temporal variation of pressure and temperature inside the tank is decomposed, using a 25-hour sliding average, to the diurnal and longer term variation (Figure 14). Compared with the amplitude of the daily variation the span of the longer term variation is larger, $\times 4$ for pressure and $\times 2$ for temperature.

The longer term variations of the radiation from radon¹ and that of pressure or temperature allow a straightforward comparison (Figure 15). The alpha and gamma sensor show a roughly concordant variation pattern, while dissimilar variation patterns are depicted by pressure (A) and temperature (B).

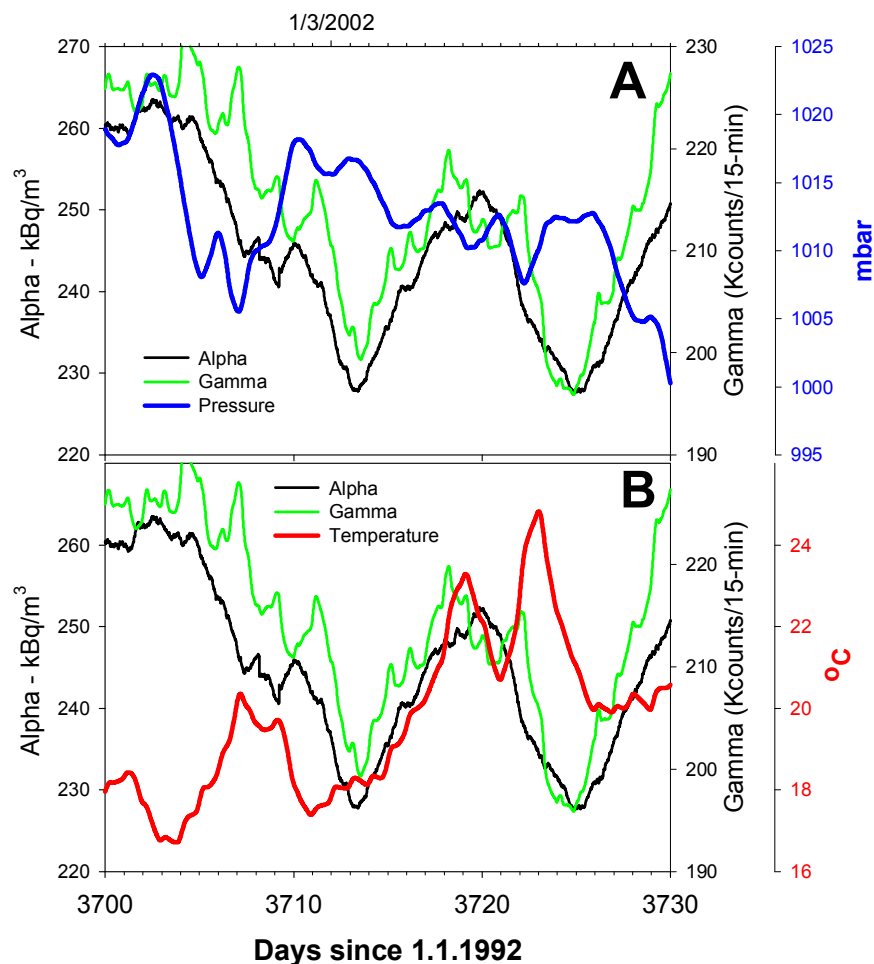


Figure 15: The longer term variation the alpha and gamma radiation inside the tank and the concurrent long term variation of internal pressure (A) and temperature (B). See text.

¹ This investigation was performed in the early phase-I, using a Barasol-MC (Algade Inc.) system with an alpha detector. In this case radon results are given in activity units, as documented at the time.

The results of these examinations of these straightforward relations among the varying level of radon in the tank and the local atmospheric factors of pressure and temperature do not support the notion of a direct connection between the temporal variation of the radon signal and atmospheric influences, and probably rather negate it.

Daily Variations

Daily Amplitude (DA)

The daily extremes of the variation, extracted from the measured signal, are used to calculate the daily amplitude (DA = "peak-to-peak") of the DR signal. Examining the temporal behaviour of the DA shows a systematic variation that differs among the sensors (Figure 16). Alpha-L exhibits a small (15% of the signal) and stable DA in time. The DA of alpha-H shows a higher variation (20-50% of the signal) that changes in time with low values around Day 5675 (=16 June 2007). The DA at gamma-C, in the order of 20% of the net gamma signal (subtracting the background radiation), also varies in time but in a different pattern – with highest values around day 5675.

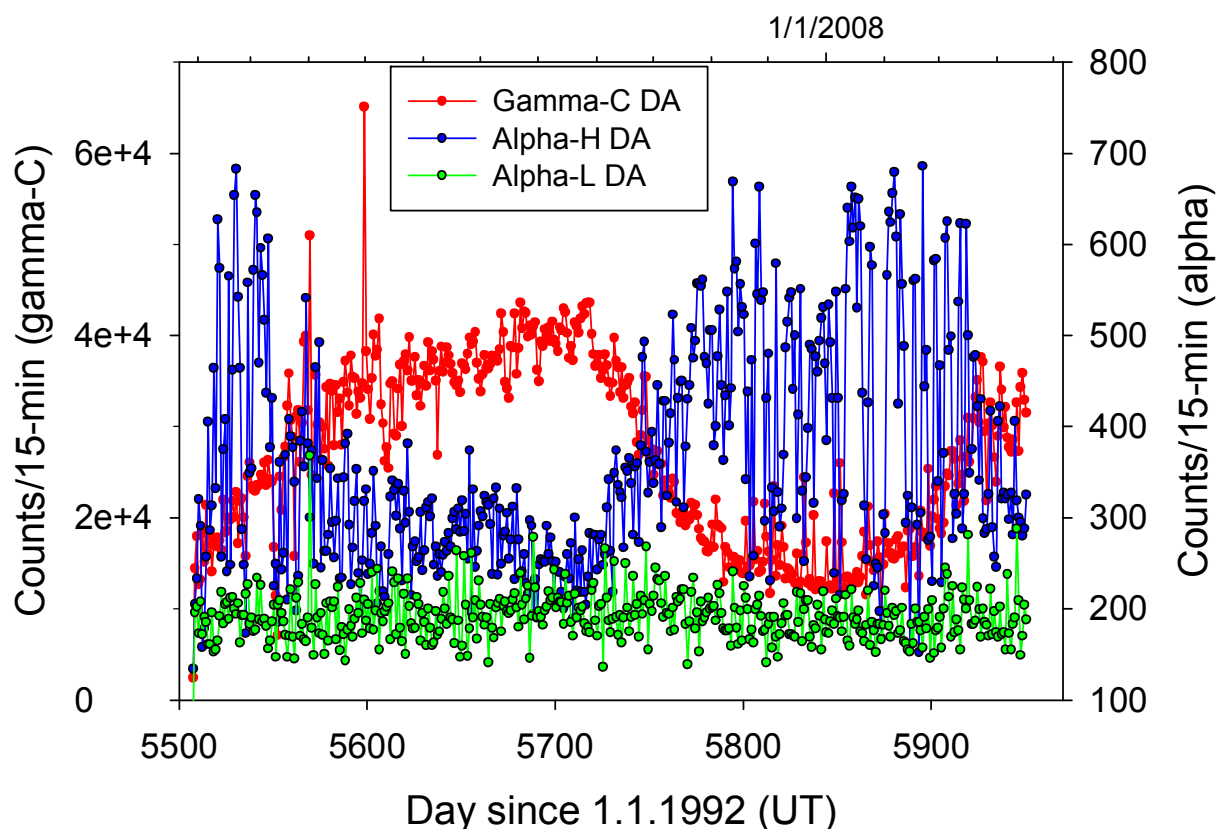


Figure 16: Temporal variation of the Daily Amplitude (DA) of the measured radon signal. See text.

This observation of a long term (seasonal) influence on DA in the system is independent of the above mentioned indication for seasonality that is based on the overall level of the measured signal. This independence stresses the significance of the opposite seasonality patterns encountered.

Periodicity - Daily Radon (DR) Signals

The overall pattern of the diurnal periodicity is investigated, using spectral analysis (Fast Fourier Transformation - FFT) of the measured signal, for the time span from Day 5525 onwards, representing the radon in the tank in the post build-up interval. Linear detrending was applied to the time series prior to the FFT analysis. The results of the FFT for the internal sensors are presented in Figure 17 per periodicities in the daily band.

The frequencies in the daily band are clearly associated with the well known solar tide frequencies S1 (24-hours), S2 (12-hours) and S3 (8-hours). Periodic components typical of gravity tide (M2, O1 etc.) are absent. The relative amplitudes of S1, S2 and S3 differ very much among the internal sensors. S1 is the strongest component in gamma-C and alpha-L. S2 is the major frequency in alpha-H, but is weak at alpha-L. The phase of these components also differs among the internal sensors and will be dealt with below.

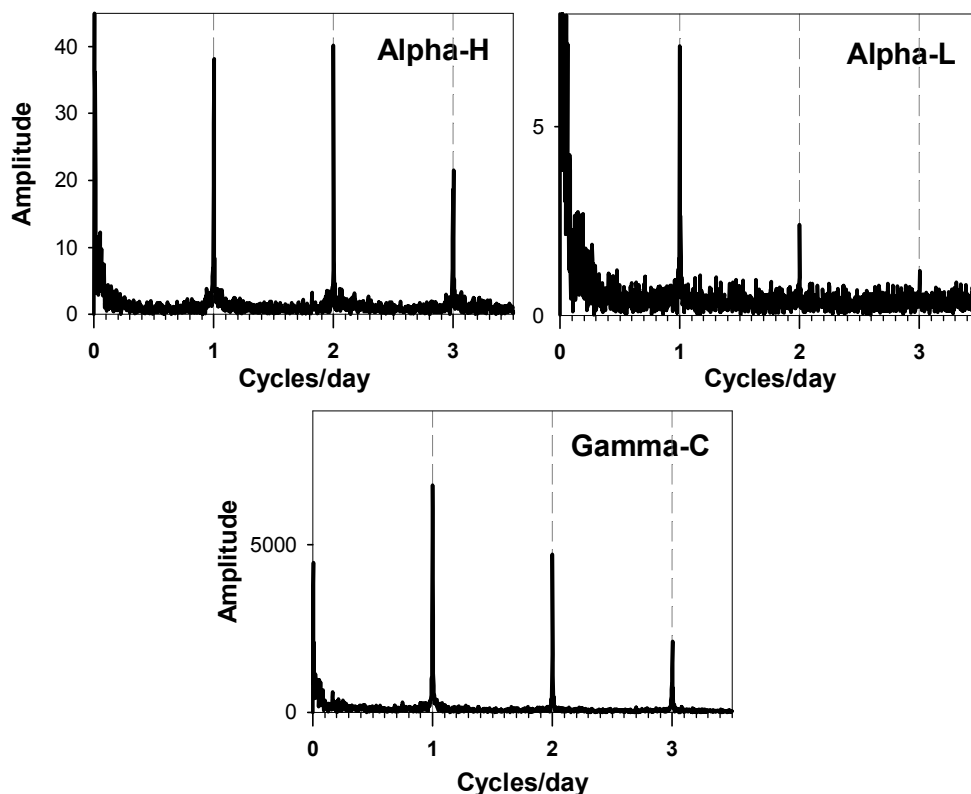


Figure 17: Spectra (FFT) of the time series (measured signal; 1-hour resolution) recorded by the internal sensors in the time interval of Days 5525-5950. Frequencies typical of S1, S2 and S3 periodicities occur in the diurnal band, exhibiting different relative amplitudes among the sensors. See text.

Temporal Patterns in the Periodic Characteristics of the DR Signal

The general characteristics of the diurnal periods, mentioned above, are further examined for temporal variation. Consecutive time intervals, 512-hour (21.323 days) long, of the measured signal with a sampling rate of 15 minutes are de-trended using linear regression, and analyzed using the FFT. Amplitude and phase of S1, S2 and S3 extracted from the respective spectra per time interval, are presented as a time series in Figure 18. Systematic temporal variation patterns observed for both amplitude and phase of the DR signal are summarized as follows:

1. The amplitude and phase of S1, S2, and S3 at alpha-H and gamma-C vary in a gradual long term and compatible fashion, per sensor. Noisy pattern are encountered in general at alpha-L, probably related to the low DR signal at this sensor. Still the stable pattern of S1 phase at alpha-L may indicate that the long term variation of the amplitude of S1 at this sensor does reflect a systematic variation.
2. The long term variations of amplitude and phase reflect an annual-seasonal influence. Opposite amplitude patterns are observed at alpha-H and gamma-C. These seasonal patterns bear a resemblance to the seasonal patterns of the daily average of the measured signal and especially to the seasonal variation of the DA (Figure 16).
3. It was shown above that the periodic components S1 and S2 are directly visible in the measured signal, mainly of gamma-C. The spectra (FFT) of long time series exhibit a considerable S3 periodicity (Figure 17). The question that immediately arises is whether this harmonic constituent is a calculation (statistical) artefact or a real physical phenomenon in the measured time series. The systematic temporal variation of the amplitude of S3 in alpha-H and gamma-C, derived from the analysis of short time intervals which are independent, indicates that this is probably a real physical feature of the measured time series. This is further supported by the conformity of the variation of S3 with that of S1 and S2.
4. The phase of S1, S2 and S3 of the diurnal periodicities differs among the internal sensors. The temporal variation patterns demonstrate the observation that the diurnal constituents of the DR signal of the alpha-H and gamma-C time series have dissimilar phase as well as dissimilar phase ratios. In the case of alpha-L a systematic phase is observed for S1, albeit the low DR signal.

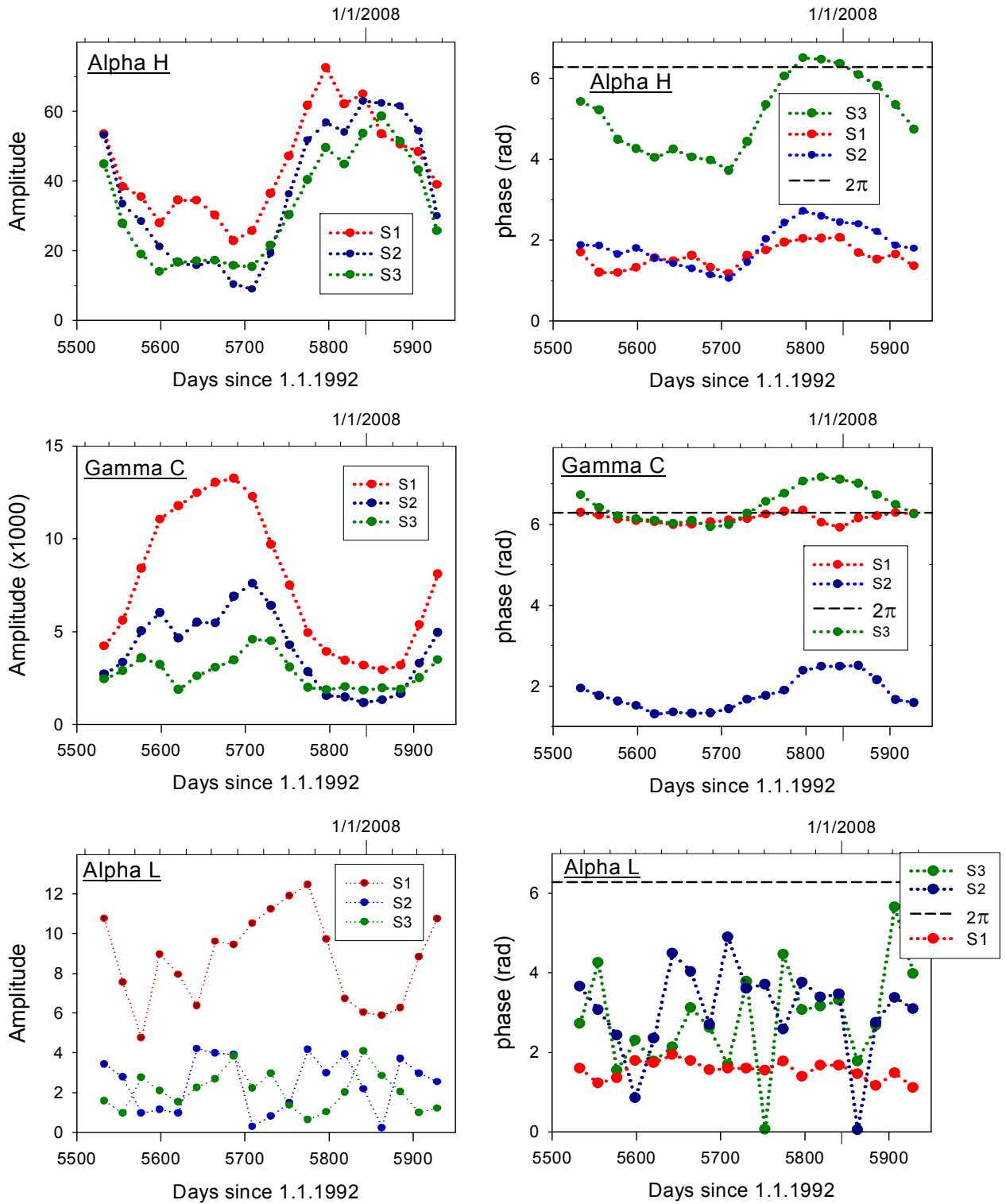


Figure 18: The temporal variation of amplitude (left) and phase (right) of the periodic DR signal measured by the internal radiation sensors. See text.

The External Gamma Radiation Pattern – Complementary Investigations (CI)

The pattern of the external gamma radiation due to radon inside the experiment tank is examined by using an external radiation source and additional detectors. The experiments (Table 3 and Figure 19) focused on gamma-ray radiation features of the phosphorite mass (CI-1,-2) and on the temporal pattern of the externally observable radiation originating from the air volume within the tank (CI-3, -4, -5). Among the latter the first short measurement interval consists of parallel measurement at gamma-W and gamma-E (CI-3). In later stages "obstructions" were placed in front of gamma-E (CI-4; CI-5; CI-5) in order to refine the understanding of the radiation pattern of the experiment.

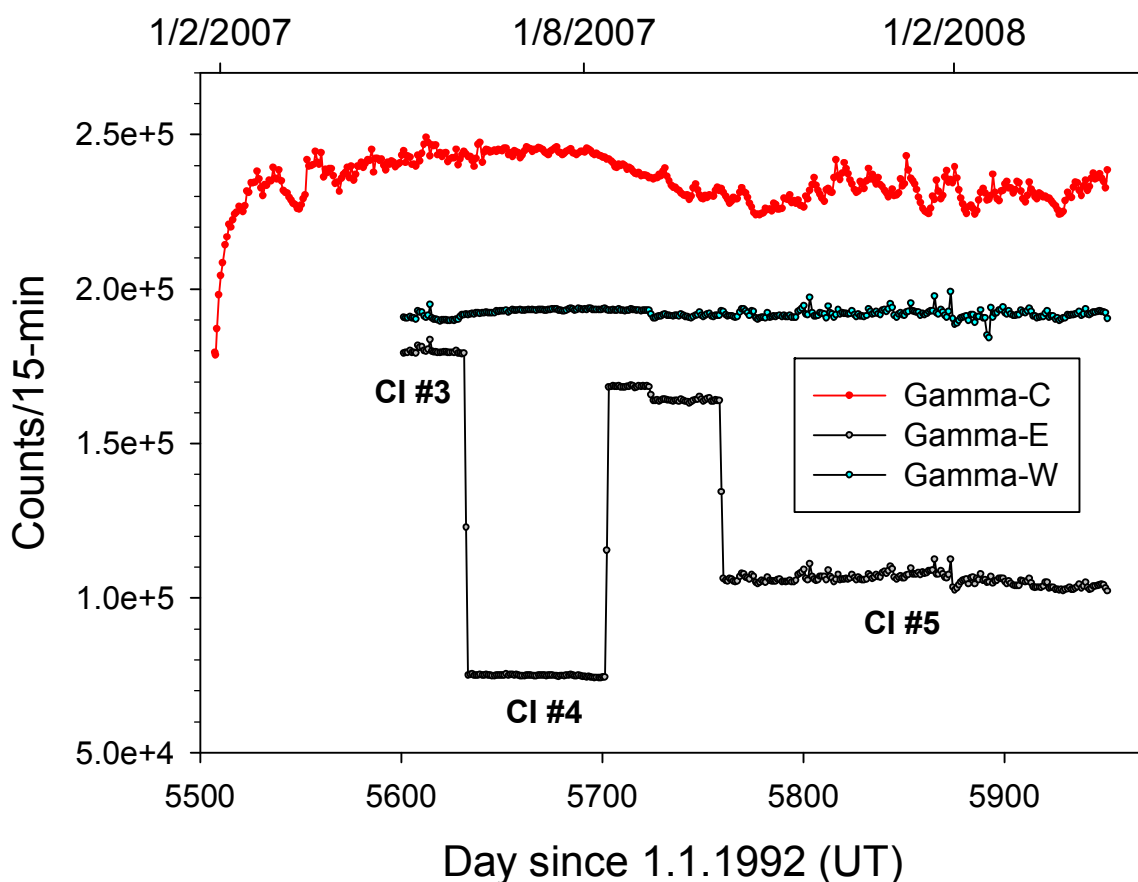


Figure 19: Time series of daily averages (DM) of the internal and external (lateral) gamma sensors. The time intervals of complementary investigations (CI) are indicated. See Table 3 and text.

Table 3: Complementary investigations (CI) around the experimental tank

CI No.	Start	End	Description and target	Figs
1	5678		<ul style="list-style-type: none"> • Influence on gamma-C of an external gamma source • Influence on gamma-C of gamma radiation from the phosphorite, as a function of depth in it 	20, 21
2	5725	5745	The pattern of gamma radiation evolving from the phosphorite	22, 23
3	5603	5632	Measuring external gamma radiation using two lateral sensors – gamma-W and gamma-E.	24-29
4	5632	5701	Blocking gamma-E sensor to the gamma radiation from the air volume in the experimental tank; Gamma-W serves as an external reference.	30
5	5761		Partial blocking of Gamma-E to the gamma radiation from the northern half of the experimental tank; Gamma-W serves as an external reference.	31-38

CI-1: Influence of an external source on gamma-C

The self shielding effect of the phosphate in the tank on the gamma-C sensor was examined by placing a relatively strong gamma source (Pitchblende ore sample) at different levels next to the front of the tank. Figure 20 shows the shielding effect of the phosphate as the source is lowered, practically blind to the gamma-C sensor at a level of 10 cm from the base of the tank.

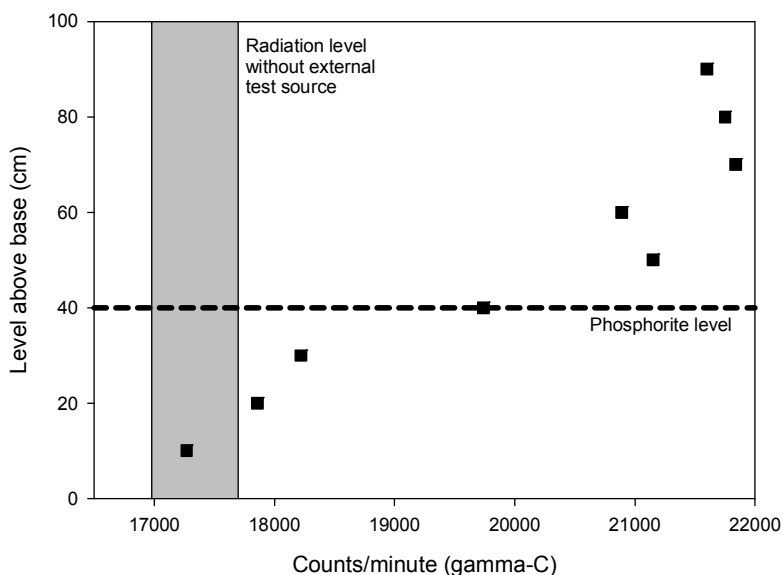


Figure 20: Influence on gamma-C of an external gamma source placed at different levels of the tank (squares).

The above result is further verified by keeping the external gamma source at the 10 cm position and performing a short monitoring experiment at a high sampling rate. The result (Figure 21) shows that placing the source at this position did not influence the variation pattern of the gamma radiation recorded by gamma-C.

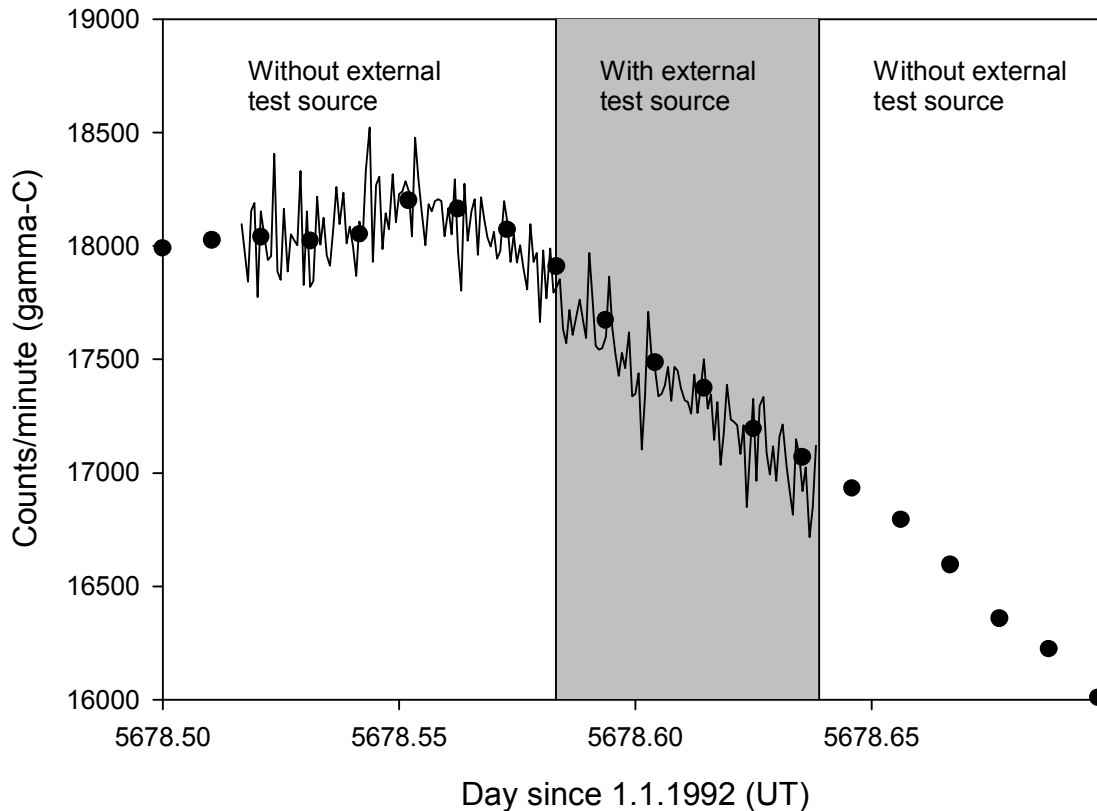


Figure 21: Influence of an external gamma source at 10 cm, activated between 14:00-15:20 hours, on the count rate of gamma-C. Sampling is at 1-minute resolution; Dots indicate the 15-minute readings.

The conclusions from these investigations (CI-1) as to the gamma-ray shielding of the phosphorite in the tank are:

- Sensor gamma-C is shielded from gamma radiation originating at a depth of more than 25 cm within the phosphorite. This complies with the expected shielding of gamma rays in soils.
- A gamma sensor placed outside and next to the tank at a level of 10 cm is practically shielded from gamma radiation originating from radon in the air volume. This conclusion will be applied below (see CI-2).

CI-2: Gamma radiation from the phosphorite

An additional external gamma sensor is placed next to the tank wall at a level of 10 cm from the bottom while covering its upper side with a 10×10×5 cm Pb shield (Figure 22). It is assumed, based on the above results (CI-1; Figure 20 and Figure 21), that gamma radiation originating from radon the air volume does not reach this sensor. Therefore it can be assumed that temporal variations recorded by this external sensor originate from radon in the pores of the phosphorite within the immediate influence zone. A 15-day long record is shown in Figure 23 along with the concurrent record by sensor gamma-C. In this interval the external gamma sensor shows a systematic decrease on which diurnal fluctuations are

clearly superimposed. These patterns reflect temporal variation of radiation from radon in the small volume of air in pores of the phosphorite. The concurrent record of gamma-C shows a similar pattern of the diurnal signal, with amplitudes larger around one order of magnitude. Notwithstanding these similarities the two time series differ considerably in terms of the shape and also the phase of the diurnal signal.

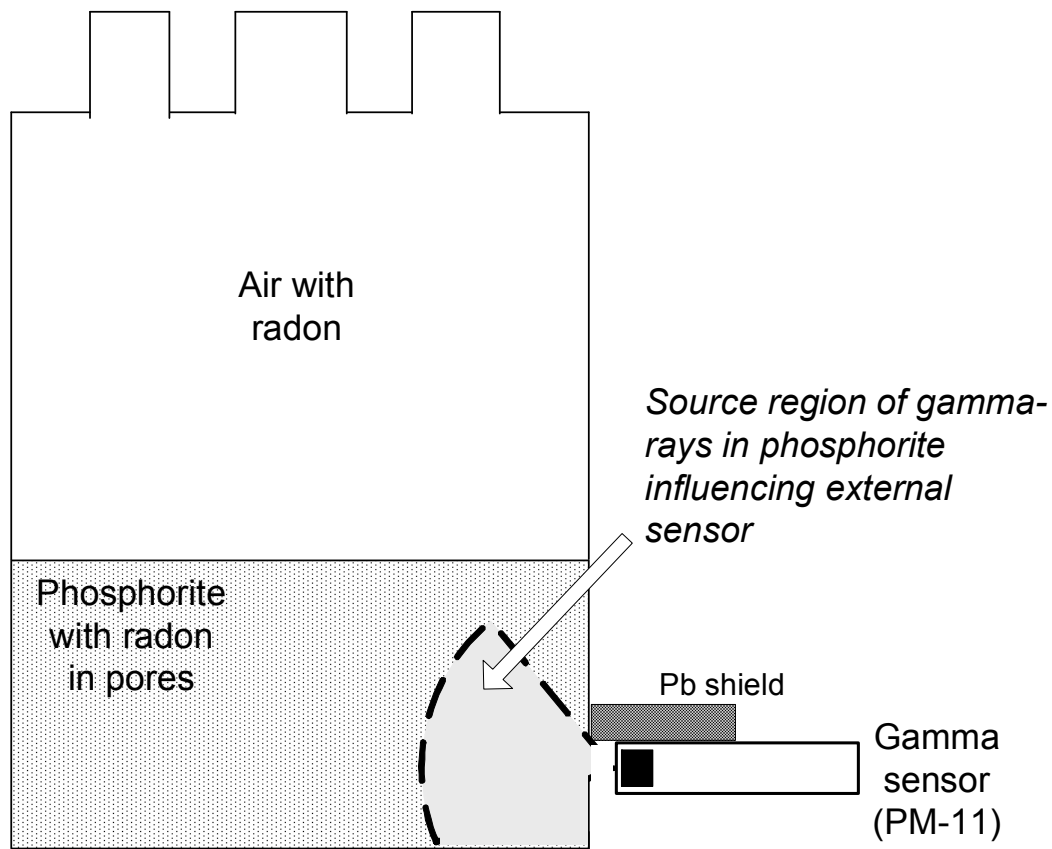


Figure 22: Layout of experimental monitoring at the phosphorite level (10 cm from bottom of tank). The zone of gamma-rays originating from the phosphorite and influencing the detector is shown, based on Figure 21. See text.

Two possibilities can be raised:

- a) The diurnal signal is generated in the air within the pores and then transferred by gas flow (advection) into the overlying air volume. This would necessitate very stable (long term) large scale gas sub-daily circulation between the overlying air volume (544 liters) and the gas phase (in the order of 50 liters) in the pores. Such a flow pattern and regime are unlikely.
- b) Radon emanated to the pores is moving out to the overlying air volume in a diffusion related/controlled mechanism. Such a pattern is difficult to visualize in terms of the fast and very regular rise rate of radiation in the Air volume. This reasoning turns impossible when one considers that there is no radon sink (in the pores or anywhere) to account for the fast and regular depletion of the apparent radon level in the Air volume.

Both options are actually implausible. Therefore it is suggested that the DR signal is generated in tandem, in all the gas phase of the tank, above the phosphorite and in its pores.

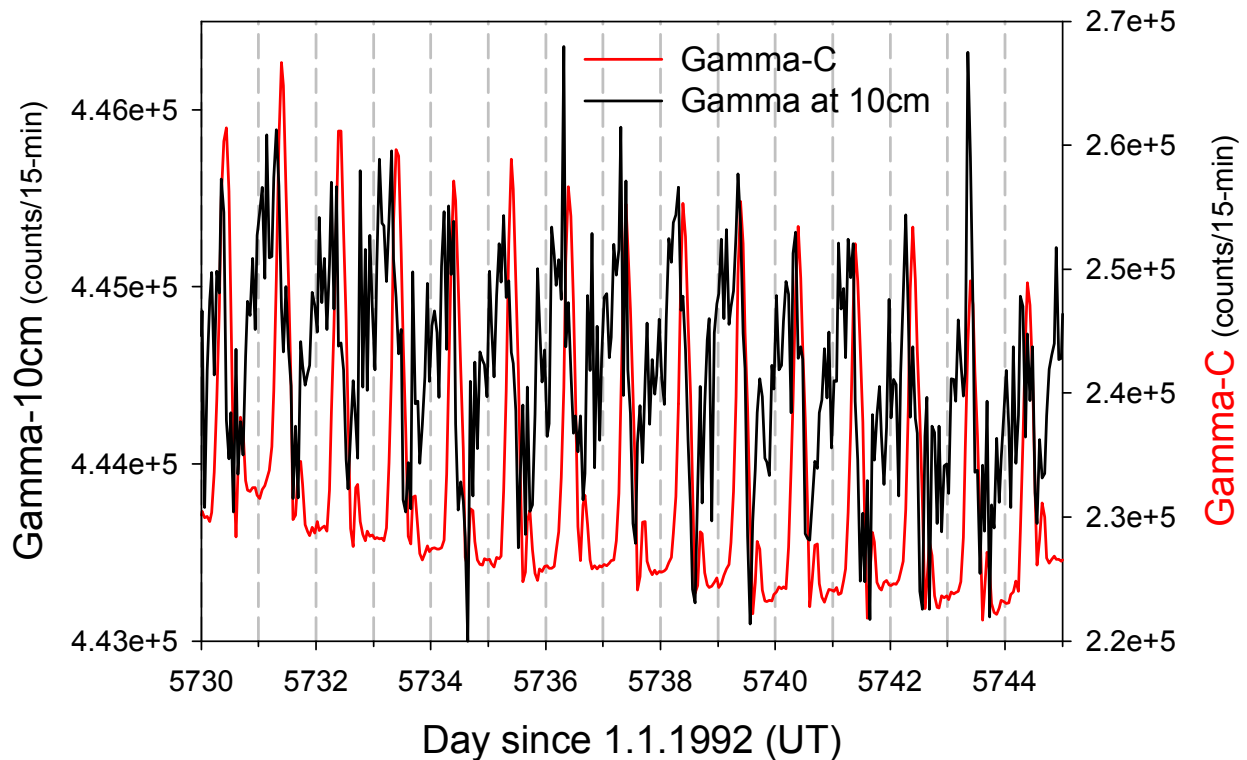


Figure 23: A 15-day record of a gamma sensor placed outside and next to the tank at a level of 10cm. Pb bricks (Figure 22) shield the sensor from gamma radiation originating in the air volume of the tank.

CI-3: Gamma radiation at two lateral sensors

Two gamma sensors are installed at lateral positions relative to the tank, roughly symmetrically on the centerline running E-W through the air volume of the tank.

Figure 19 shows the overall relation among the time series of the daily averages recorded by the internal and external gamma sensors. Referring to the unobstructed pattern of gamma-W it is noticed that a long term variation is barely visible (see below).

Further insight is obtained by looking at hourly averages shown in Figure 24 for a 30-day long interval, and in higher detail in Figure 25 and Figure 26. The main features observed at the lateral gamma detectors are:

- a) Multi-day (MD) signals apparent in the time series of gamma-C are lacking in the record of the lateral gamma. The latter exhibit other MD signals (see below; CI-5).
- b) Small periodic diurnal fluctuations – DR signals. The amplitude of the concurrent DR signal at gamma-C is larger by factor $\times 10$;

- c) Short non-periodic signals – Sub Diurnal Radon (SDR) signals. Considering the symmetric lateral position, relative to the tank, of the two sensors and the extremely high concordance of these SDR signals it is concluded that they originate from the tank. On the other hand such SDR signals do not occur in the record of the internal gamma-C (nor in the record of the alpha detectors);

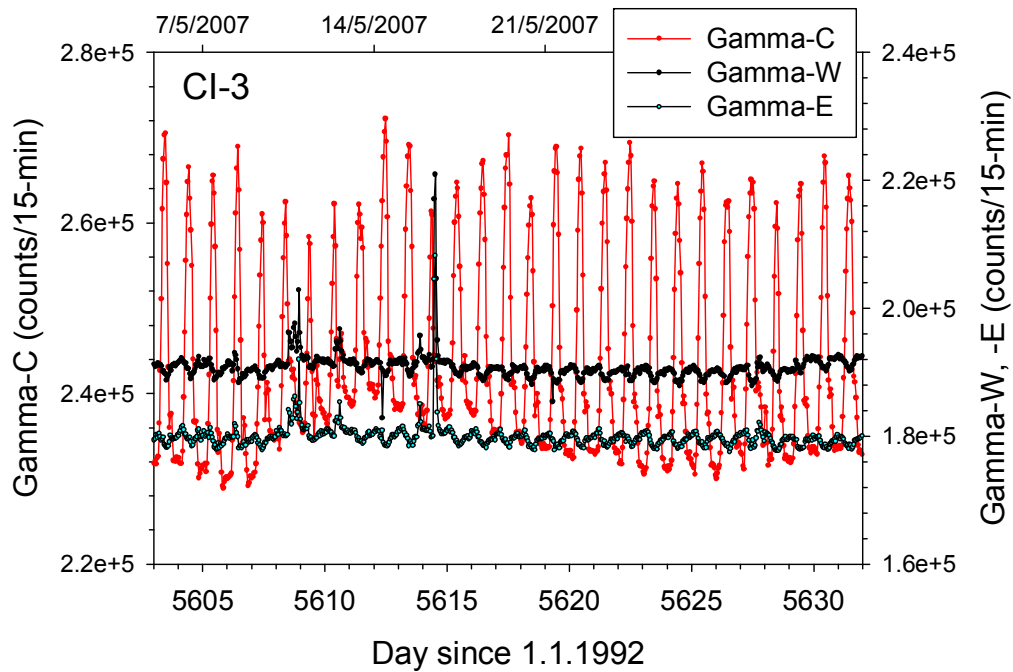


Figure 24: Time series from the lateral gamma detectors showing: a) similar overall levels; b) superimposed periodic Daily Radon (DR) signals and c) non-periodic short Sub Diurnal Radon (SDR) signals. The concurrent time series of gamma-C is also shown, exhibiting DR signals with $\times 10$ amplitudes. MD signals are apparent only in the record of gamma-C.

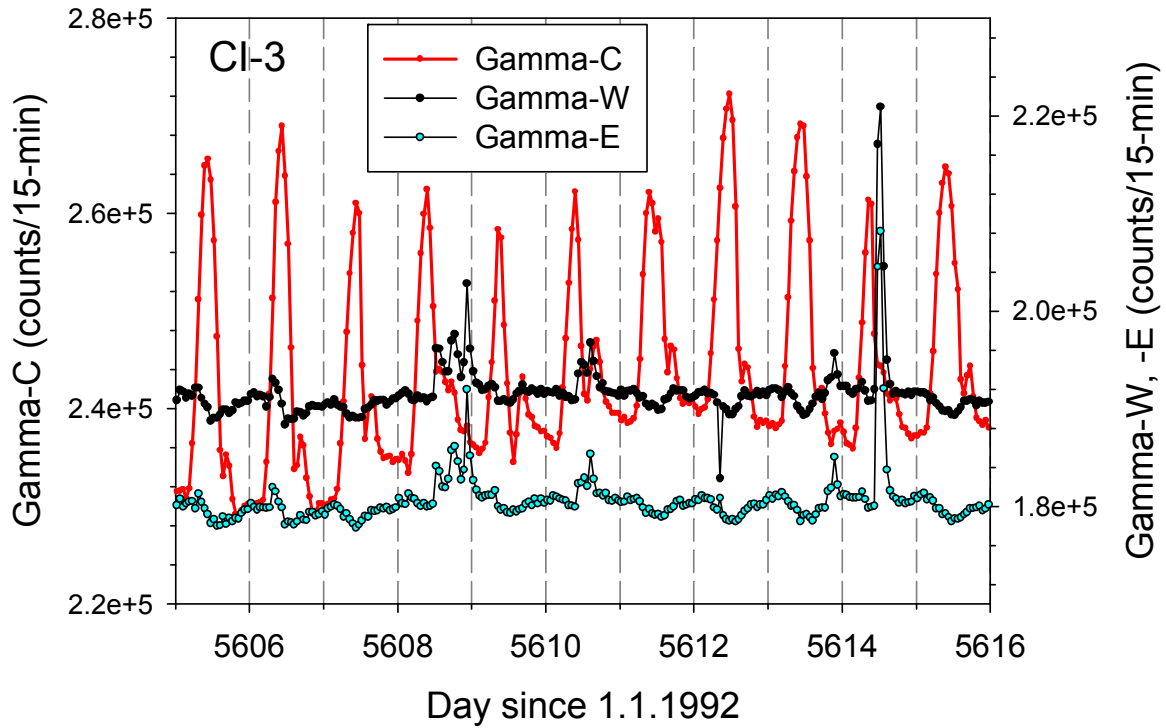


Figure 25: Detail of Figure 24. The non-periodic short Sub Diurnal Radon (SDR) signals are very similar in the record of the lateral gamma detectors, but do not appear in the record of gamma-C

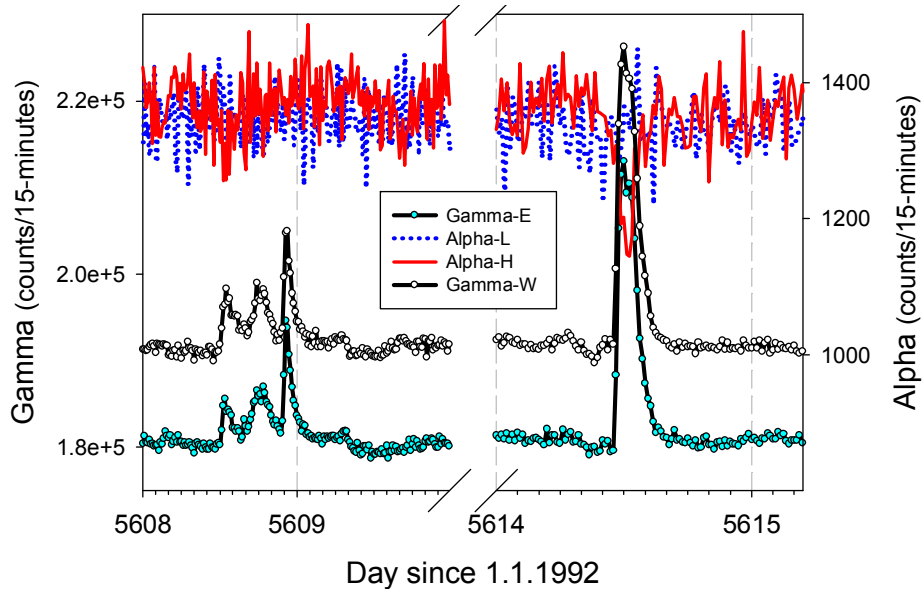


Figure 26: Detail of SDR signals recorded by the external gamma sensors. The high concordance of these signals indicate that the source is located in a position which is symmetrical to both sensors. In one case a related response possibly occurred at alpha-H.

The direct implication from these observations is that the external sensors are recording a signal pattern which is both related and different from that recorded by the internal gamma sensor. The overall level of radiation is of similar scale. Periodic signals (SR, DR) seem to be relatively smaller as the overall level at the external sensors. On the other hand only the external sensors record the SDR signals.

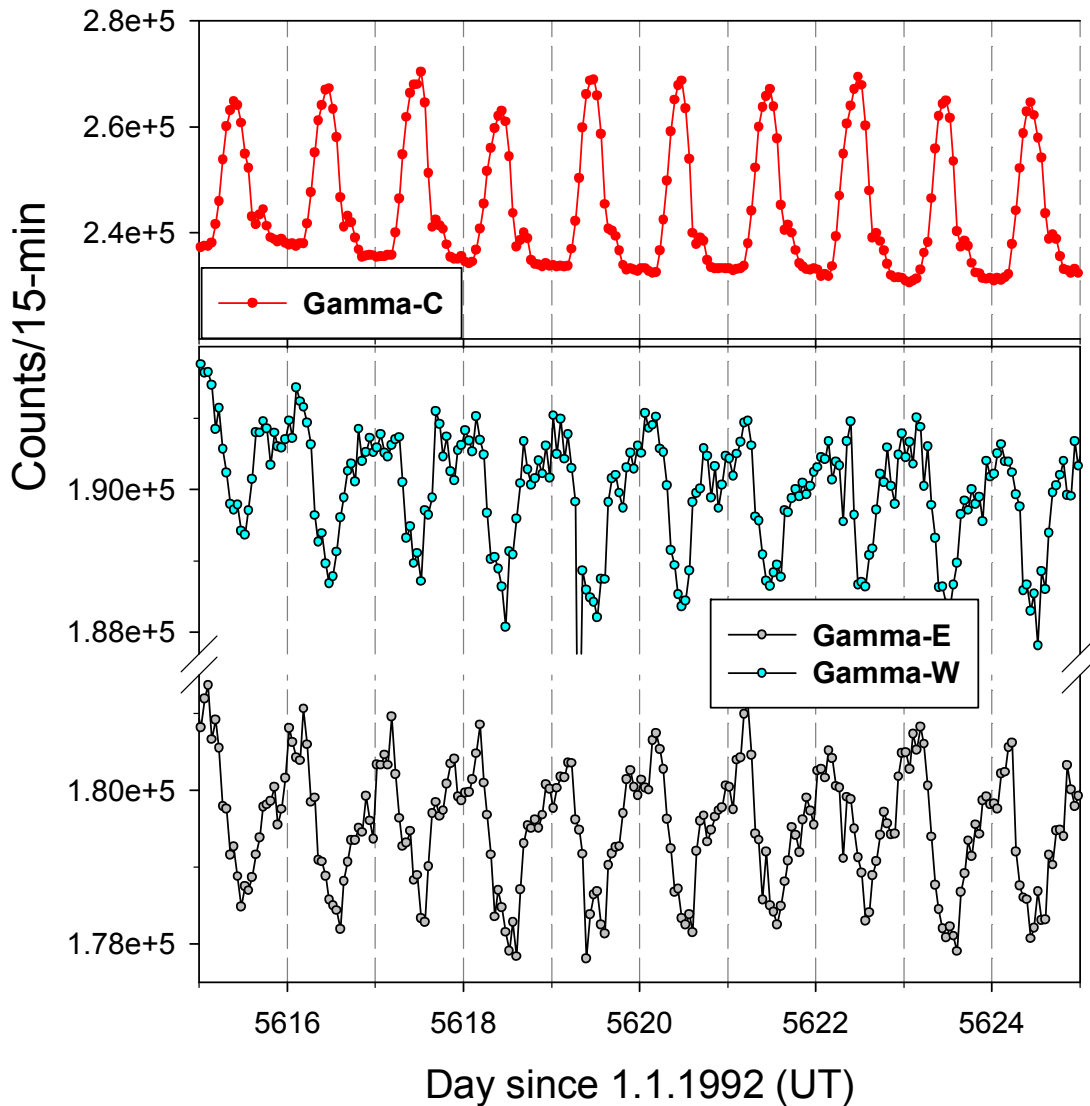


Figure 27: A 10-day interval of the record of the measured signal from the two external gamma sensors flanking the tank, compared with the synchronous record from the internal gamma-C. The two external sensors show a DR signal that is approximately in phase, and in anti-phase with gamma-C. A semidiurnal component is apparent in all three cases. 1-Hour resolution. See text.

Daily Radon (DR) signals occurring in the time series from the gamma sensors are compared in Figure 27. The amplitude of lateral DR signals is of similar magnitude but an order of magnitude lower than the amplitude of DR signals recorded by gamma-C (0.4×10^5 vs. 0.3×10^4 counts/15-minutes). This is in difference with the aforementioned similarity in the overall gamma radiation level among these sensors (25% difference; Figure 19). Furthermore, the two opposing external sensors show concordant fluctuations, which are

different from the trend exhibited by gamma-C. Comparing these signals with those of the gamma-C shows that:

- The DR signal exhibits a very different phase
- The DR signal of gamma-C is relatively sharp (smaller FWHM = Full Width at Half Maximum) compared to the signal of the external sensors. This may be connected to the fact that gamma-C is placed within a Pb tube.

The picture evolving from these observations is that the DR signal is manifested in similar patterns at the two lateral sensors, which are in a roughly symmetric position to the system, and in a different pattern at the central sensor.

The diurnal periodicity of the external gamma-W and the internal gamma-C sensors are demonstrated with their spectra during days 5601-5950 (Figure 28). The typical diurnal periodicities S1 and S2 that occur inside the tank are also recorded by the lateral sensors, at reduced intensity ($\times 10$).

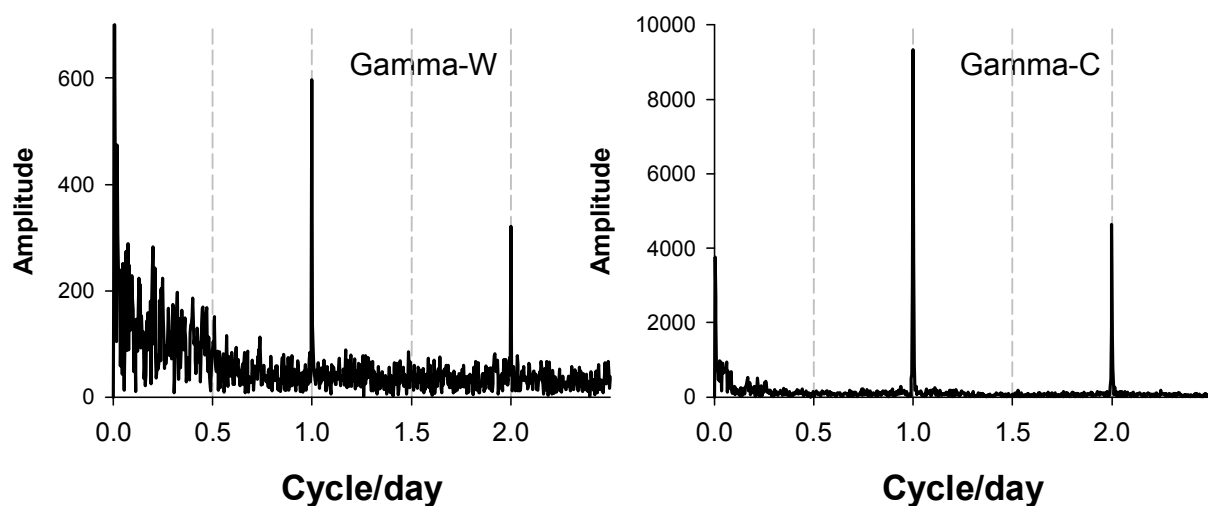


Figure 28: Spectra of the records of an external gamma sensor (gamma-W) and the internal gamma sensor (gamma-C), during 350 days (measured signal; 1-hour resolution). Periodicities S1 and S2 are clearly observed also at the external sensor, but with different relative amplitudes.

The temporal variation of the amplitude and phase of the diurnal constituents of gamma-W is shown in Figure 29. Compared with the pattern of gamma-C (Figure 18) the pattern of gamma-W is noisier. Still seasonality is probably indicated in the amplitude of S1.

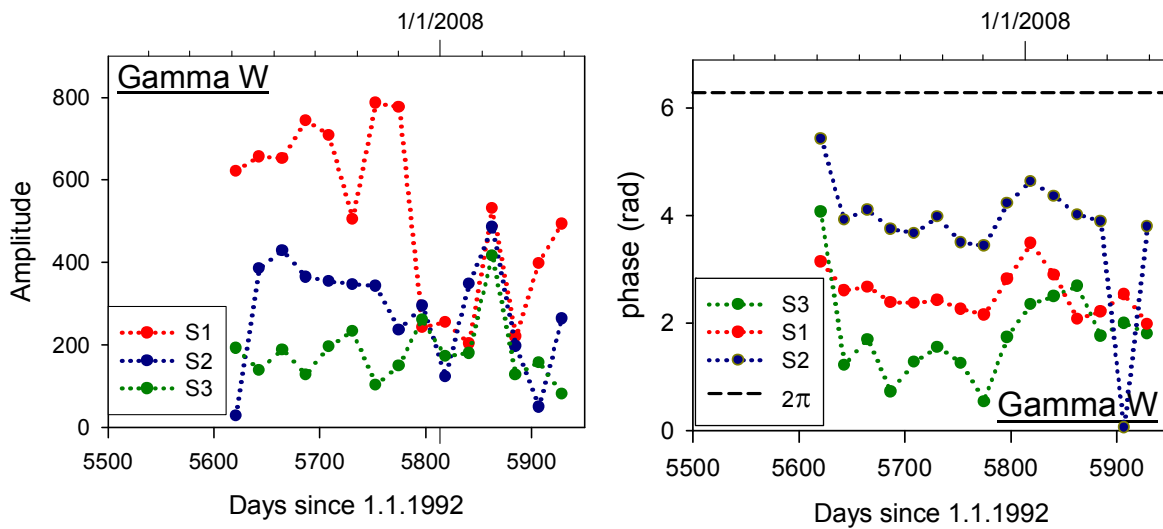


Figure 29: The temporal variation of amplitude and phase of the diurnal periodic variation measured by sensor gamma-W. See text.

CI-4: Blocking gamma radiation from the air volume of the tank

A 20×20×5 cm lead shield is placed in front of the gamma-E sensor (see Figure 1) practically blocking the gamma radiation reaching from the air volume in the tank while enabling only part of the radiation emanating from the phosphorite region of the tank. The obtained level of radiation of 75 kcount/15-minute is somewhat lower than the bulk background gamma radiation observed in the tank (85 kcount/15-minute; Vulkan et al., 1998). Diurnal fluctuations are observed, originating from the air within the pores of the ground phosphorite (Figure 30). The amplitude of the diurnal signals at gamma-E is around 1 kcount/15-minute vs. 2 kcount/15-minute at gamma-W. The DR signal shows a similar phase in both environs within the tank.

It is difficult to account for the fast variation rates of these DR signals and their conformity by diffusion and/or advection between the regions in the tank. Therefore the conclusion from these observations is that DR signals are generated in the air in pores of the phosphorite and in the air volume in the upper part of the tank.

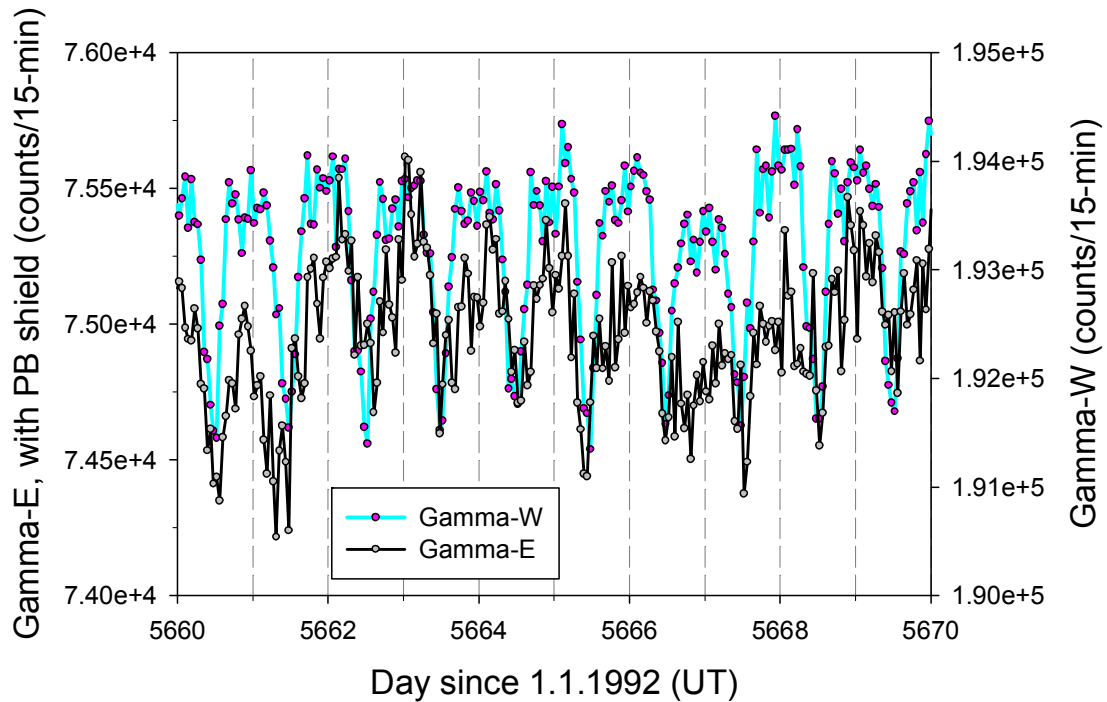


Figure 30: A 10-day interval of the record from gamma-E sensor with a 5 cm thick Pb shield in front, blocking the direct radiation from the air volume of the tank. 1-Hour resolution. See text.

CI-5: Blocking gamma radiation from the northern half of the tank

Further tracking of the complex external radiation pattern is examined by blocking sensor gamma-E from the radiation emanating from the northern half of the eastern face of the experiment. This is achieved by placing a vertical Pb shield in front of northern half of gamma-E (Figure 31). This configuration blocks half of the bulk gamma radiation evolving from both phosphorite and the air volume, assuming an overall conforming radiation field.

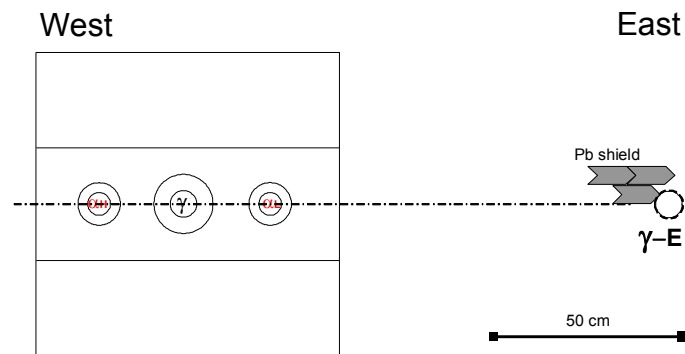


Figure 31: Topview of experimental setup during CI-5, using 10×10×5cm Pb bricks to shield gamma-E from radiation originating from the northern half of the tank (detector gamma-W is not shown).

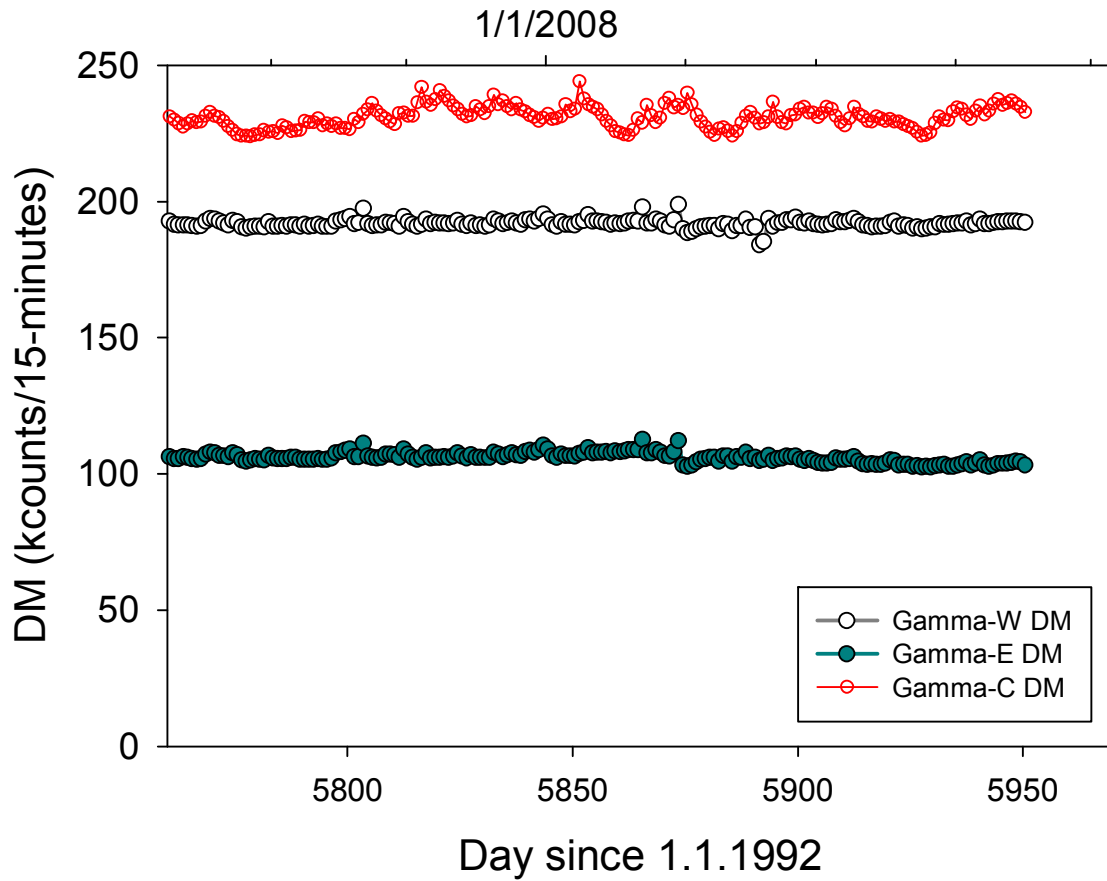


Figure 32: Time series of the Daily Mean (DM) of the lateral gamma sensors and gamma-C during CI-5 interval, with the partial blocking of gamma radiation to gamma-E. The overall level of radiation at gamma-E is reduced. See Text.

The overall patterns and statistics of the variation of the signal in this interval (CI-5) at the lateral detectors and the internal gamma-C are summarized below.

Table 4: Statistics of daily variation at the two external and the internal gamma detectors

		gamma-W	gamma-C	gamma-E
Daily Mean (DM)	Average	194,826	230,994	105,908
	StDev	1,517	3,938	1,847
Daily Amplitude (DA)	Average	5,428	19,540	4,546
	StDev	6,597	6,345	5,340

As expected the overall effect of this partial blocking configuration, presented in Figure 32 using the DM, is lowering the radiation level recorded by gamma-E to around 50% compared with that measured at gamma-W (compare Figure 19). The long term seasonal variation pattern observed at gamma-C (Figure 5) is also apparent at gamma-W and by the partially blocked gamma-E (Figure 33). In spite of the large difference in the overall level between gamma-E and gamma-W it is striking that the overall intensity of the seasonal variation in both sensors is of similar magnitude, both of them around half the variation in gamma-C. In other words the overall lowering of the radiation level at gamma-E does not affect (lower) significantly the variability of the DM.

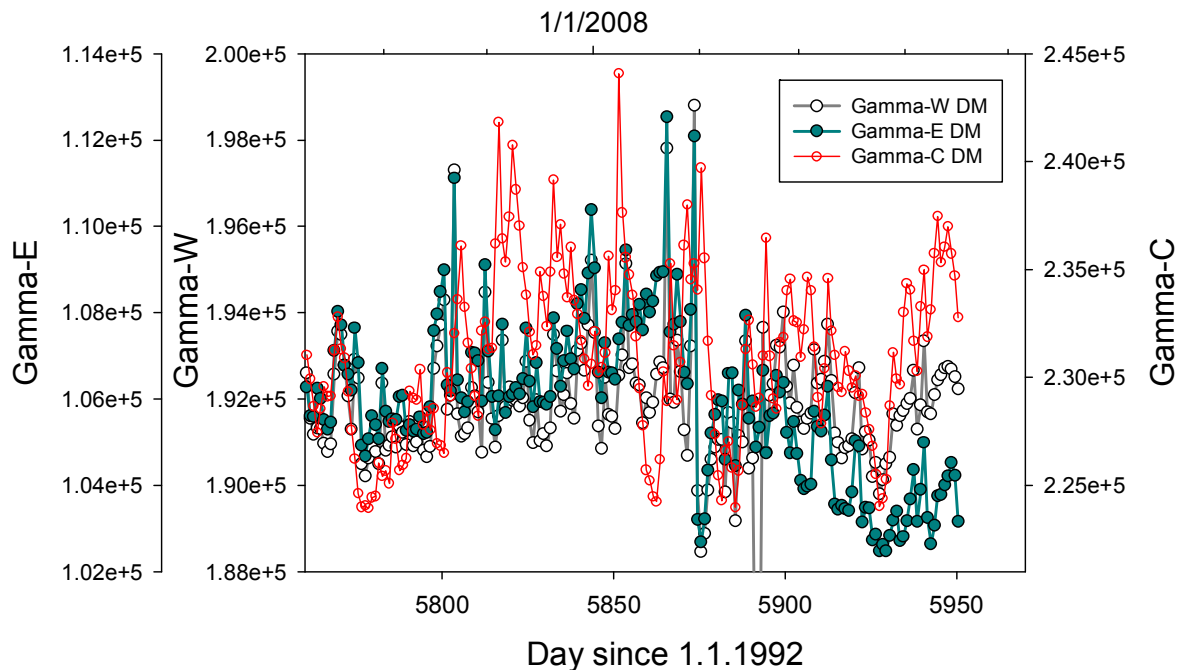


Figure 33: Detail of Figure 32 exhibiting the apparent seasonal pattern in the DM time series of the lateral gamma sensors, compared to the internal gamma-C. The vertical scale of the lateral sensors is 50% of the scale for gamma-C. Multi-Day (MD) variations are superimposed on the seasonal variation. See text.

The last mentioned discrepancy is further revealed when considering the Daily Amplitude (DA). The seasonal variation pattern, shown above for the DA of gamma-C (Figure 16), does not occur in the time series of the lateral gamma detectors (Figure 34), which exhibit a similar long term pattern. Short term fluctuations of the DA are superimposed on all three time series. Some of these fluctuations are very strong, especially in the case of the lateral sensors. The fluctuations of the DA in the gamma-C time series do not correlate with fluctuations in the DA time series of the lateral sensors. On the other hand, the two lateral gamma sensors, situated on opposite sides of the tank, exhibit a very high correlation of the DA (Figure 35).

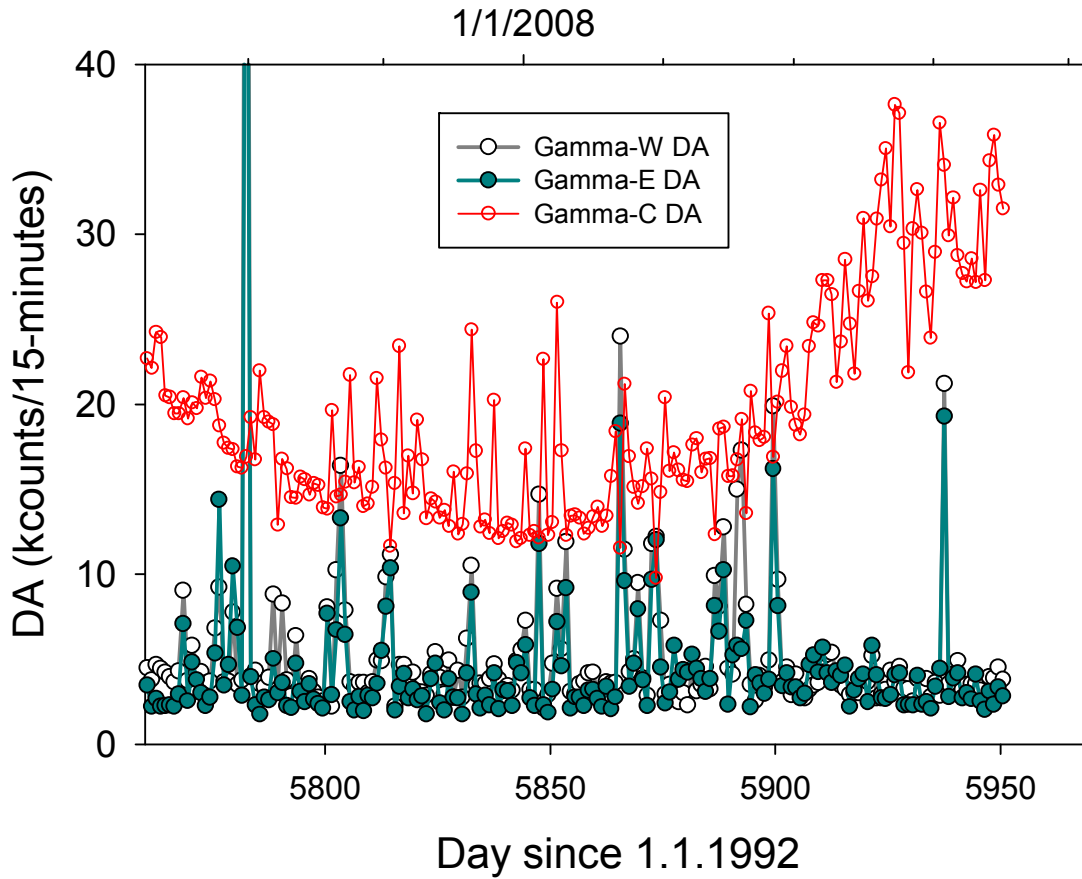


Figure 34: Time series of the Daily Amplitude (DA) of the lateral gamma sensors and gamma-C during CI-5 interval, with the partial blocking of gamma radiation to gamma-E. See text.

The direct implications from these observations on the temporal pattern of the DM and the DA are that: a) the lateral sensors see a similar radiation pattern which is consistent with their symmetric position relative to the tank; b) the radiation patterns at gamma-C differs from the radiation pattern at the lateral gamma sensors, and c) these differences are reflected in long- and short term signals.

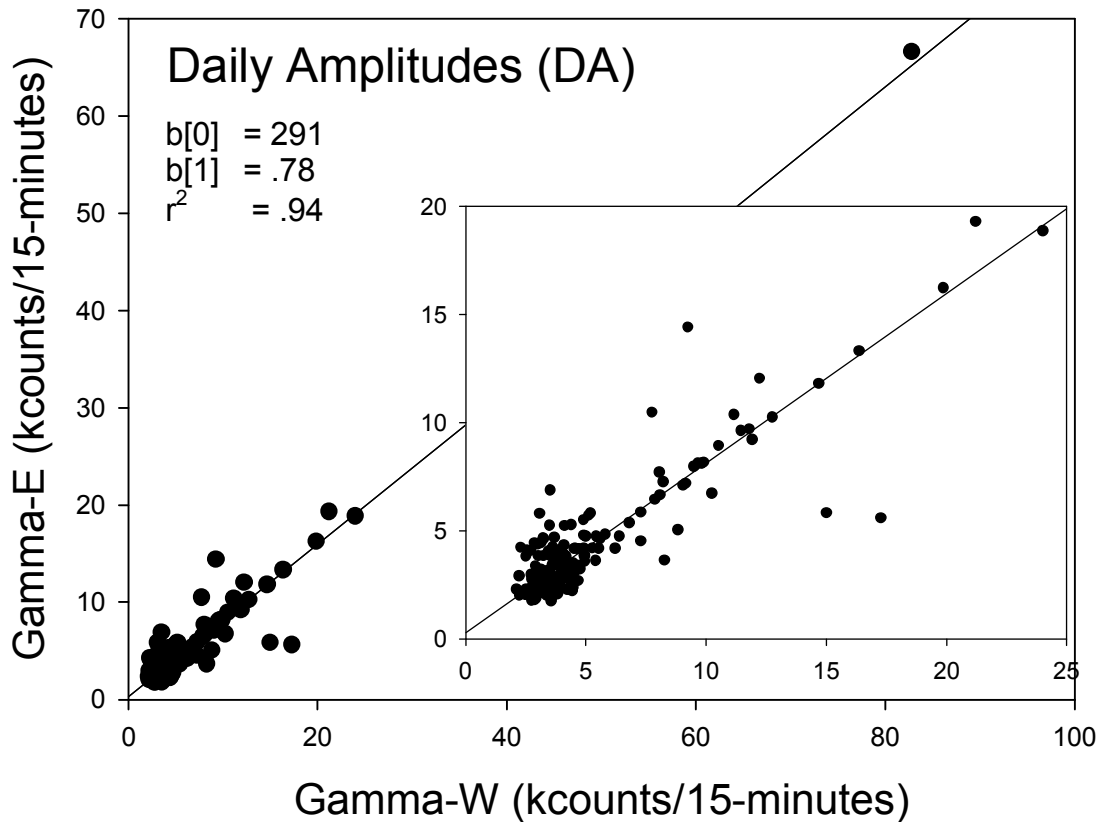


Figure 35: Correlation diagram of the Daily Amplitude (DA) among the lateral gamma sensors during CI-5 interval, with the partial blocking of gamma radiation to gamma-E.

Multi-Day signals occur in the time series of the lateral sensors. The overall effect of the partial blocking of gamma-E on these signals is examined for a 60-day time interval in Figure 36-A by filtering (FFT) and reconstructing a time series in the interval of 2-30 days (0.5 to 0.03333 CPD). Both detectors, roughly located symmetrically to the tank, exhibit highly concordant MD patterns. The concordance in the amplitude of the MD variation stands out further considering the overall reduced level of radiation at gamma-E. The result of an identical analysis of the concurrent signals in the time series of the three internal sensors is also shown in Figure 36-B. The internal sensors show generally similar patterns, which are different from the MD pattern of the external sensors.

These results augment the last mentioned conclusions by allowing to infer that the radiation pattern in the tank experiment and its immediate surrounding is non homogenous but related in both the spatial and time dimension. The outcome of this is that the record at each sensor depends, among other things, on its geometrical location with the setup.

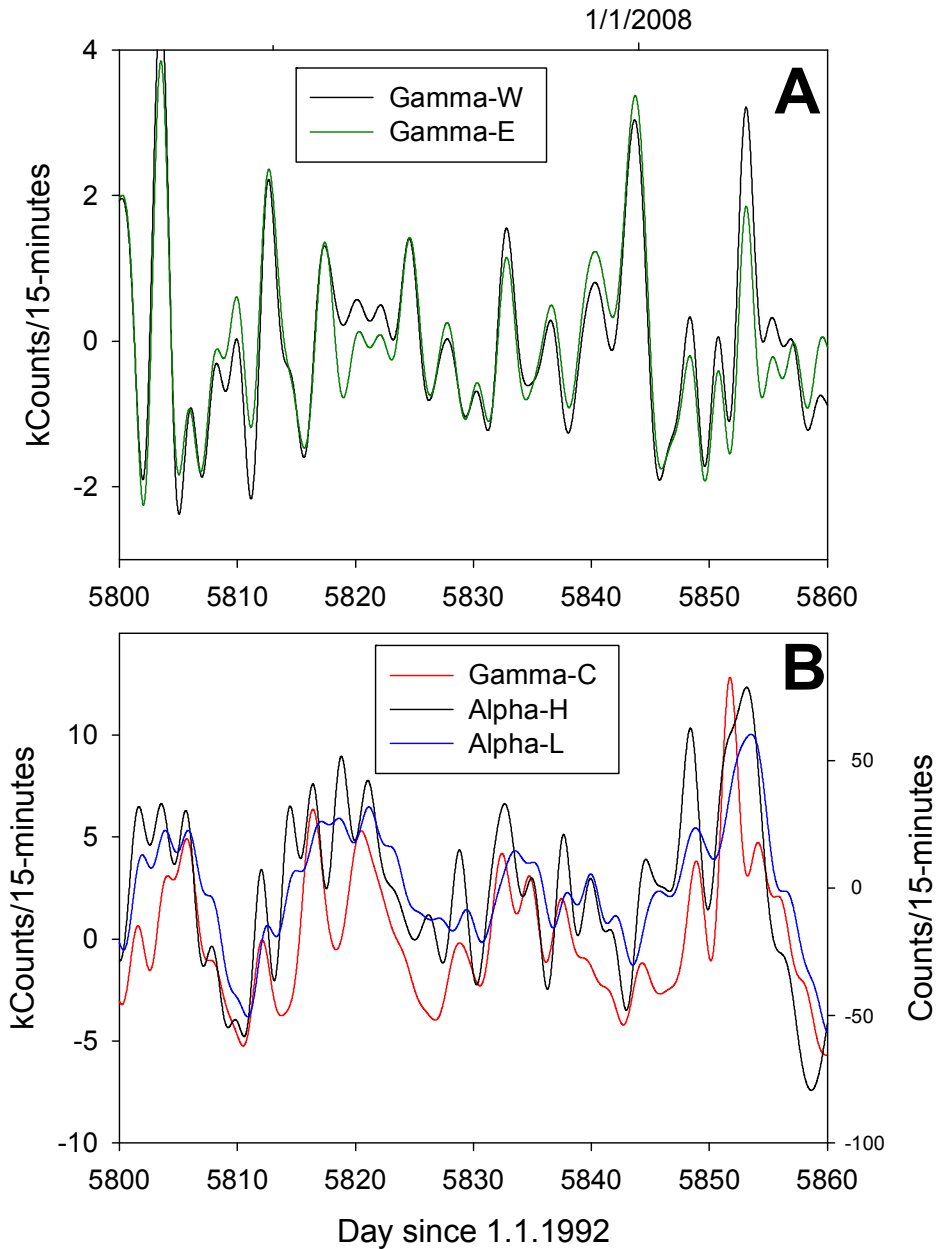


Figure 36: Multi-Day (MD) variation patterns during CI-5 interval.

A – Variation pattern in the time series of the lateral gamma sensors

B – Variation pattern in the time series of the internal sensors.

See text.

The response of the two external gamma sensors to the radiation from the tank is further elaborated by addressing the DR signal in Figure 37. This 20-day interval shows a concordant MD variation, as in Figure 36-A. On the other hand the periodic DR signal occurs with a significantly reduced intensity (50%) at gamma-E, shown in more detail in Figure 38.

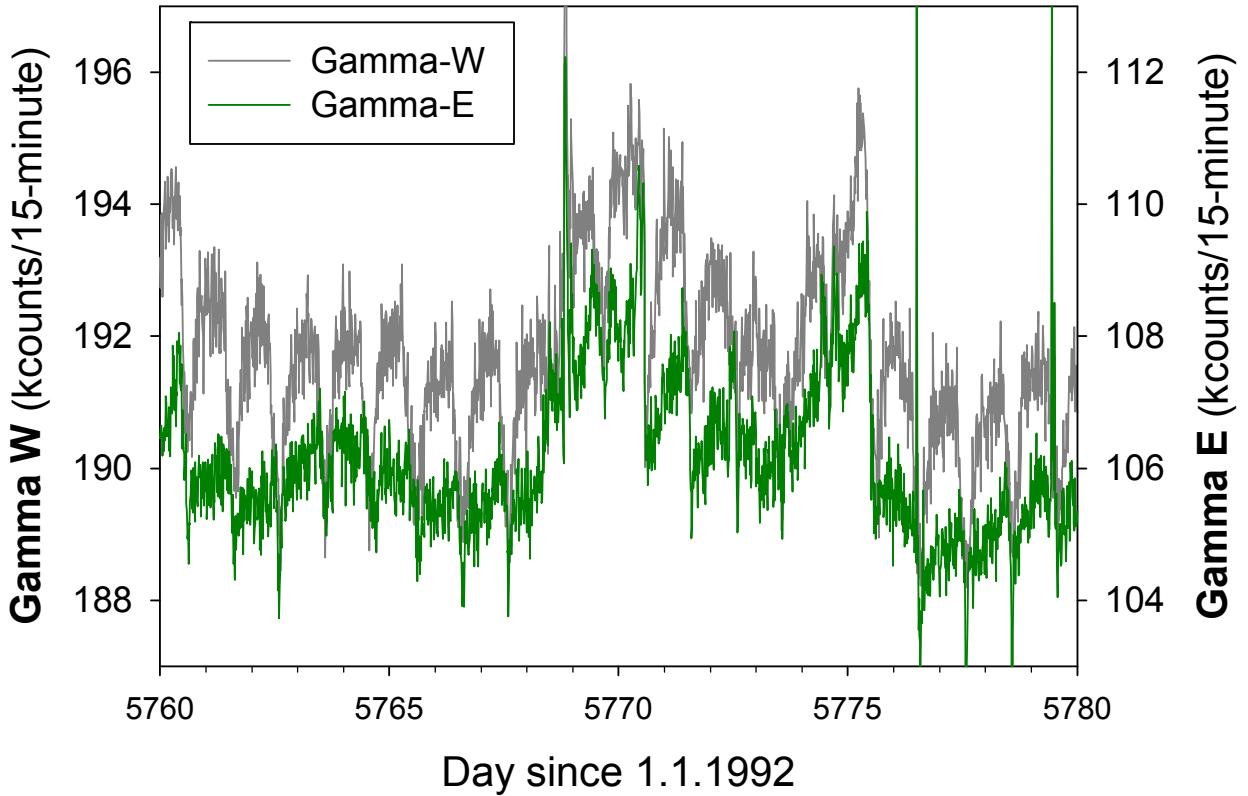


Figure 37: A 20-day long time series of the measured signal of the lateral gamma sensors during CI-5 interval, with the partial blocking of gamma radiation to gamma-E. The net scale for both sensors is 10 Kcounts. The MD signals reflected in both sensors are concordant and with very similar intensity. The DR signals are reduced to around 50% in gamma-E. See Text.

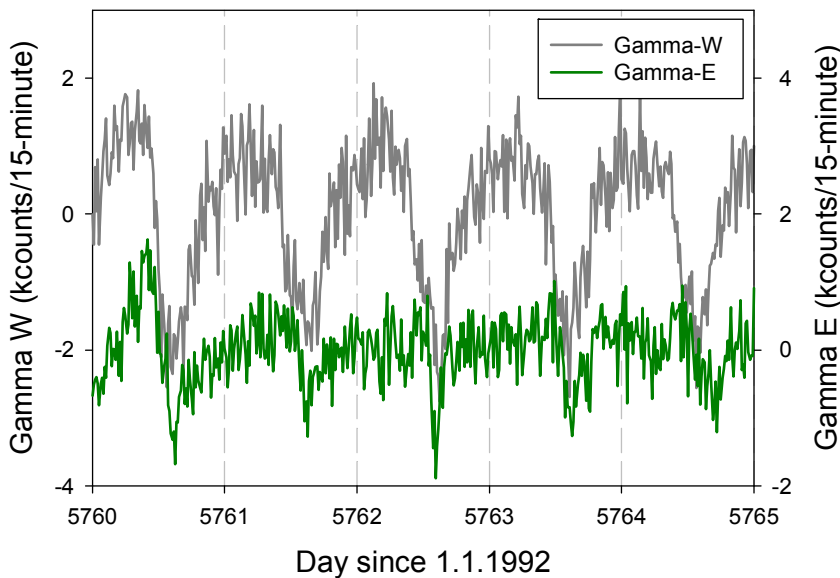


Figure 38: Detail of the DR signal (after decomposition) at the external gamma detectors. Note the reduced signal (~50%) at gamma-E. See text.

The results of CI-1 to CI-5 are summarized as follows:

In terms of the gamma radiation pattern the lateral detectors observe a similar bulk radiation level which is symmetric to the experiment and 20-25% less than that recorded by gamma-C. The gamma radiation is emanating from a source in the phosphorite and from the overlying air volume. Blocking half of the facility (50% of the phosphorite and 50% of the air volume) to an external sensor halves the bulk radiation reaching it.

The two lateral gamma sensors exhibit similar characteristics of the temporal variation pattern, as expected from their symmetric position relative to the experimental system. On the other hand, depending on signal type these characteristics are similar, dissimilar or partly similar to those recorded by the internal sensors (primarily gamma-C).

The temporal variation of the daily amplitude (DA) of the lateral gammas reflects well their symmetric position relative to the system. This well correlated pattern is retained even when the bulk radiation is halved by partial (vertical) blocking of the radiation. A long term SR signal is encountered at the lateral sensors, similar to the pattern in gamma-C but with a halved scale of variation. Blocking half of the bulk radiation does not further lower this variation. The SR pattern of the DA of gamma-C (and alpha-H) is absent in the time series of the DA of the lateral gamma sensors. All in all these features point to some sort of inhomogeneity and profound differences between the internal and external radiation pattern.

Very similar multi-day (MD) signals are recorded by the two lateral sensors, with forms alike those encountered inside. Notwithstanding the latter resemblance, the temporal pattern of external MD signals is dissimilar to the pattern of internal MD signals, which are concordant among the three internal sensors (alpha & gamma). The picture is further complicated by the observation that the intensity of very similar MD signals at the two lateral sensors are not affected by halving the bulk radiation. All this hints, at face value, that the overall radiation pattern over the experiment is symmetric in E-W direction and asymmetric in terms of the inside-outside bearing.

The daily radon (DR) signal is formed (generated) in tandem in the gas phase within the pores of the phosphorite and in the air in the upper volume, i.e. it is not transferred (moved) from the phosphorite to the overlying air volume or vice versa. In difference to the similar level of the bulk radiation the amplitude of the DR signal is lowered by a factor $\times 10$ at the lateral gamma sensors relative to the amplitude at gamma-C. A further lowering of 50% of the amplitude occurs when the bulk radiation is halved. These differences in the manifestation of the DR signal within and outside the tank are further supported by the similarity of form and phase relations among the external sensors, compatible with their symmetric positioning, and their difference with the phase and form of the internal gamma-C.

Sub-daily radon (SDR) signals are encountered in a highly concordant pattern only at the external gamma sensors. This can maybe indicate that this signal is determined and directed by the geometric edges (boundaries) of the radiation source, i.e. the geometric edges of the volume containing radon in the gas phase of the experiment.

Discussion

The experimental setup simulates situations in the natural geological environment. Radon is emanating from a natural rock source into a local gas system which is in a confined environment and in ongoing contact with the rock system. Furthermore, the setup is located close to the shallow subsurface level and is influenced by the local environmental conditions. The source of the radon in the gas phase of the experiment is from the Ra-226 in the phosphorite, from which about ~12% emanates into the gas. Secular equilibrium between Ra-226, the emanated radon (Rn-222) and its radioactive decay in the gas phase is attained after build-up lasting around 20 days, as expected. The alpha detectors in the tank record alpha particles due to the decay of radon in the gas phase in the immediate vicinity of the sensor (cm scale). The gamma sensors record gamma radiation evolving from a much larger volume which includes the topmost 20 cm of the granulated phosphorite and the air, primarily in the upper volume of the tank and also in the porosity of the phosphorite. The gamma radiation is composed of two components – that emitted from radioactive isotopes in the decay series of U, Th and K in the solid, and that emitted from the decay of radon in gas components. While the gamma radiation from the solid phase is constant the radiation from radon in the gas phase of the tank varies.

The initial observations collected while the experimental tank was located at SNRC, using observations lasting up to several tens of days, in the years 1996-2003, are confirmed after relocating and installing the setup at the GSI in 2007, and using a new set of sensors. These relate primarily to the signal types and variation patterns recorded by the internal sensors, to the observed phase shift of the DR signal, as well as to the non-direct relation of these to local atmospheric conditions.

The assumption and expectation is that once secular equilibrium is attained within the tank stable and uniform alpha and gamma radiation patterns will be observed. In contrast the observations imply non uniformity within and outside the tank of the radiation field in both the spatial and temporal dimensions. The different, systematic and large variations of the measured signals are in disagreement with the anticipation. In general two primary causes could be raised to explain the observed variation patterns:

- a) exchange of radon between the tank and the external environment;
- b) environmental-atmospheric influences;

Initially, the setup of the experimental system was not intended for the investigation of these issues. Still, the two alternatives are negated on the following grounds.

Being a noble ultra-trace component in the gas system selective transfer of radon atoms between the internal and external surroundings is not possible. Thus exchange of radon between the tank and the external atmospheric patterns requires large scale transfer and circulation of significant portions of the air mass via leaks in the system. This cannot be reconciled with the mechanical structure of the tank system, nor with the systematic patterns of variation.

The experiment (second phase), performed under an open shack, is evidently influenced by local climatic atmospheric conditions. Barometric pressure variations are passed into the tank via the thin walls and likely minute leaks. This and especially differences in thermal properties of parts of the system (different wall sides, phosphorite mass in lower part etc.) certainly force advection and convection within the enclosed gas system. The effect of such perturbations is to enhance the mixing of the gas system contained in the tank. Thus a

homogenous and stable radon level is expected within the isolated experimental setup. In this configuration it is difficult to see how external atmospheric variations generate large diurnal variations in the concentration of radon within a small and homogenized air volume. Furthermore, the experimental testing performed during phase-I showed that pressure and temperature variations cannot account for the observed signals, and certainly cannot account for the apparent concentration differences recorded among the sensors at the daily scale.

Radiation encountered at different points within and around the experimental setup indicates spatial and temporal in-homogeneity of the radiation field. Thus the overall characteristics and several lines of consideration suggest that other processes interact to form the observed patterns.

Taking the observations at face value the alternative option that so far unrecognized processes are involved in the generation of the unique radiation patterns is evaluated below. The main properties of the space-time radiation pattern are:

- a) They are due to radon and its daughters in the gas phase of the system, primarily in the air volume above the phosphorite but also in the air within the pores of the phosphorite.
- b) They are reflected by alpha radiation from decaying radon-222 (half-life of 3.82 days) and polonium-218 (half life of 183 seconds), and by gamma radiation due to the decay of Pb-214 (half-life of 26.8 minutes) and Bi-214 (half-life of 19.9 minutes).
- c) Dissimilar radiation patterns among alpha and gamma sensors appear to be related to the geometric position of the sensors relative to the experimental setup.
- d) Temporal variations are superimposed on the equilibrium level, at amplitudes of up to several tens of percent.
- e) Some of the fluctuations are below the equilibrium value (Alpha-H) indicating an apparent deficit.
- f) Temporal variations are of periodic and non-periodic nature and occur at sub daily to annual-seasonal scale.
- g) Periodic variations are observed in the time and frequency domain and in the time-frequency domain.

Systematic temporal variations of the radiation signal are:

1. Long term variations due to an annual-seasonal variation pattern the SR signal.
2. Multi-day variations (MD signal) which occur in a non-periodic manner.
3. Periodic daily radon (DR) signal, with typical periodicities of S1, S2, S3.
4. Short, sporadic and non-periodic sub-diurnal radon (SDR) signal.

The fluctuations in the radiation, which are beyond the level expected at secular equilibrium, originate from the radon in the gas phase. Taking into account the amount of the fluctuations (tens of percent) the fast rates of change cannot be accounted for using conventional terms and scales of release, diffusion, decay, absorbance or leakage of radon - a noble ultra-trace gas component in the isolated air of the experimental setup. The conclusion is that these variations do not reflect changes in the concentration (number of atoms per unit volume) of radon in the gas system, but rather only "apparent" or virtual changes in concentration. It is therefore suggested that variation in radiation level is due to different and unidentified processes and interactions. These account for both increase and also decrease of the radiation relative to that expected at the equilibrium level.

The observation that periodicity is so prominent in the variation of the radiation implies an external influence on this process. A priori, periodicity is not expected to be present in the radioactive signal originating from the radon in the air in the confined volume of the tank. In spite of this all three internal sensors record strong and similar periodicity. Frequencies S1, S2, typical of influences due to the rotation of the earth around its axis, dominate the daily frequency band. The lack of periodicities typical for tidal (gravity; M2, O1) influences – which are due to lunar effects – indicates that the observed periodicities of S1-S2-S3 are rather due to the influence of “solar tide” or solar irradiance.

The periodic variations must be due to an external influence on the system. Profound connections between the seasonal and daily variation are found, in the time and frequency domains. Seasonality is forced or induced on several modes and features of the radon signal:

1. It occurs in the measured signal of two (out of three) internal sensors, in a conformable pattern
2. It occurs in the temporal variation of daily amplitude (DA) of two of the internal sensors, but in a distinct inverse fashion
3. It arises in the temporal trend of the amplitude of S1, S2, & S3 of two internal sensors in inverse fashion, and
4. It arises in the temporal trend of the phase of S1, S2, & S3 of two internal sensors.

Excluding point 2 & 3 these manifestations are independent of each other. Combining these observations implies a strong interconnection between the seasonal and diurnal patterns. This in turn again implies a mutual connection with the rotation of Earth around its axis and its rotation around the sun. This leads to the proposition that an element in solar radiation is involved.

Lacking an obvious reason for an internal process the generation of MD and SDR signals probably is also due to external forcing.

The external periodic and non-periodic forcing leads to diverse interactions inside the tank. The resulting radiation pattern is reflected at the sensors with a dependence on the location of the sensor, relative to the geometry of the tank system. The main geometric elements of the experimental system are the tank itself and the mass of phosphorite and the volume of the overlying air. As mentioned the external drivers must be of a very distant source. The influence-reflection of a varying irradiance related distant driver should lead to similar and homogenous temporal patterns at the sensors. Generation of local differences in the radiation pattern necessitates that a further secondary and limited interaction occurs. This secondary interaction, which is related to the dimensions of the experimental system, drives the local variation patterns. An obvious candidate for this interaction is the phosphorite mass. It may well be that a specific quality of the phosphorite is involved in the local process generating the secondary interaction which drives in turn the radiation from radon in the gas phase. The possibility is raised that the mineral lattice plays a role in the interaction with the external driver. This role of the phosphorite is in addition to being the source of the radon.

The evolving scheme of interactions and the suggestion that the phenomena are related to the nuclear radiation from a decaying radioactive atom in the gas phase is further strengthened if one considers that alpha radiation is due to the decay of Rn-222 and the decay of Po-218 while gamma radiation is due to the decay of Bi-214 and Pb-214.

A recent study of the radon phenomenology in the Elat Granite and its statistical characteristics (Steinitz et al., 2007; Barbosa et al., 2007) demonstrated and suggested that:

- a. Large and non-linear variation patterns existing in radon time series cannot be accounted for in the subsurface regime by simple and direct time varying processes in the gas system such as emanation, diffusion, absorption and advection.
- b. Negation of above surface atmospheric influences, in particular pressure and ambient temperature
- c. Seasonal, MD and DR signals compose the variation.
- d. Periodicity in the DR signal is characterized by S1 and S2 periodicities, implying an external above surface driving mechanism.
- e. The latter feature combined with the lack of tidal gravity periodicity led to suggesting the influence of a process related to solar radiation on the DR signal and also the seasonal variability.

This outline derived for the Elat Granite is in accordance with observations from further locations in Israel and elsewhere. The observations and conclusion from the herein described experimental investigation are comparable and inline with phenomena of the temporal behavior of radon in subsurface geogas.

So far the understanding of the complex behavior of radon in geogas is lacking a comprehensive framework. This investigation shows that characteristics of phenomena observed in radon from the natural subsurface environment can be mimicked using an experimental setup. The results herein, combined with recent ones from the natural environment, present a few far reaching propositions:

- The phenomena cannot be explained using conventional terms of diffusion, advection combined with radioactive decay. They rather pose a contradiction to them.
- So far such phenomena are observed only in the case of the radon system, a noble radioactive gas, and its immediate daughters also in the gas phase. This suggests a link to the radioactive behavior of radon in the gas phase.
- The link to radioactive properties is also supported by the observation of non-uniform spatial-temporal alpha and gamma radiation features – which is not expected in this case.
- It is proposed that an external influence related to solar irradiance interacts with the radon system, homogenously dispersed in the gas phase, leading to radiation at spatially preferred directions.
- Accepting influence of an external driver, the driver must be interacting with the nucleus of the radon in order to generate preferential orientation of the radiation (the generation of which is a nuclear process).

These propositions pose a new prospect and frame for understanding the involved processes.

Implications

This is a first laboratory verification of phenomena of temporal variation observed in the natural subsurface environment which are unique to radon. This example should serve as a basis for further investigations of the involved processes by:

- Maintaining and running the present experimental setup to serve as a reference laboratory time series of the phenomena, as long as no alternative is established;
- Advance further experiments to be performed in two complementary and parallel modes - experimentation in the laboratory and at selected field sites.

Acknowledgements

Early phases of activity that led to this experiment were conducted while the experimental setup was located at the Soreq Nuclear Research Center (SNRC; Yavne). SNRC staff members Uzi Vulkan (deceased), Yaacov Assael, Yoav Yaffe, and Gustavo Haquin participated and helped. Colleagues at the GSI contributed at various stages: Naama Gazit, Uri Malik, Meirav Bass, Peter Kotlarsky and Sara Erlich.

Different versions of the report benefited from discussions with Hovav Zafrir, Zeev B. Begin and Susana Barbosa.

This study was supported by the Israel Science Foundation (Grant no. 524/05) and by the Earth Science Administration of the Ministry of National Infrastructures (Grants no. 26-17-009, 27-17-025).

References

- Alparone, S., Behncke, B., Giammanco, S., Neri, M. and Privitera, E., Paroxysmal summit activity at Mt. Etna (Italy) monitored through continuous soil radon measurements, *Geophys. Res. Lett.*, 32, L16307, 2005. doi:10.1029/2005GL023352
- Aumento, F., "Radon tides on an active volcanic island: Terceira, Azores. *Geofísica Internacional*, 41, 499-505, 2002.
- Balogh, B. and Steinitz, G., Radon monitoring at the Gavnunim site, Makhtesh Ramon. Interim Report. *Isr. Geol. Surv. Tech. Rep. TR-GSI/22/04*, 17p., 2004.
- Ball, T.K., Cameron, D.G., Colma, T.B. and Roberts, P.D., Behavior of radon in the geological environment: a review. *Q. J. Eng. Geol.*, 24, 169-182, 1991.
- Barbosa, S. M., G. Steinitz, O. Piatibratova, M. E. Silva, and P. Lago (2007), Radon variability at the Elat granite, Israel: Heteroscedasticity and nonlinearity, *Geophys. Res. Lett.*, 34, L15309, doi:10.1029/2007GL030065.
- Begin, Z.B. and Steinitz, G., Temporal and spatial variations of micro-earthquake activity along the Dead Sea Fault, 1984-2004. *Israel Jour. Earth Sci.*, 54, 1-14, 2005.
- Burton, M., Neri, M. and Condarelli, D., High spatial resolution radon measurements reveal hidden active faults on Mt. Etna. *Geophys. Res. Lett.*, 31, L07618, 2004.
- Cigolini, C., Salierno, F. Gervino, G., Bergese, P., Marino, C., Russo, M., Prati, P., Ariola, V., Bonetti, R. and Begnini, S., High-Resolution Radon Monitoring and Hydrodynamics at Mount Vesuvius. *Geophys. Res. Lett.*, 20, 4035-4038, 2001.
- Finkelstein, M., Eppelbaum, L.V., Price, C., Analysis of temperature influences on the amplitude frequency characteristics of Rn gas concentration. *J. of Environ. Radioactivity*, 86, 251-270, 2006.
- Hartmann, J. and Levy, J. K., Hydrogeological and gasgeochemical earthquake precursors - A review for application. *Nat. Hazards*, 34, 279-304, 2005.
- Imme, G., La Delfa, S., Lo Nigro, S., Morelli, D. and Patane, G., Soil radon monitoring in the NE flank of Mt. Etna (Sicily). *Appl. Radiat. Isotopes*, 64, 624-629, 2006.
- Monin, M.M., Seidel, J.L., Radon in soil-air and groundwater related to major geophysical events: a survey. *Nuclear Instruments and Methods in Physics Research. Section A: Accelerators, Spectrometers, Detectors and Associated Equipment*. 314 (2), 316-330, 1992.
- Pinault, J.L., Baubron, J.C., Signal processing of diurnal and semidiurnal variations in Radon and atmospheric pressure: a new tool for accurate in situ measurement of soil gas velocity, pressure gradient, and tortuosity, *J. Geophys. Res* (102) 18,101-18,120, 1997.
- Reddy, D. V., Sukhija, B. S. , Nagabhushanam, P. and Kumar, D., A clear case of radon anomaly associated with a micro-earthquake event in a Stable Continental Region. *Geophys. Res. Lett.*, 31, L10609, 2004. doi: 10.1029/2004GL01997
- Richon, P., Perrier, F., Sabroux, J.-C., Trique, M., Ferry, C., Voisin, V., Pili, E., Spatial and time variations of radon-222 concentration in the atmosphere of a dead-end horizontal tunnel. *J. Environ. Radioactivity*, 78, 179-198, 2005.
- Segovia, N., Mena, M., Seidel, J.L., Monnin, M., Tamez, E., Pena, P., Short and long term radon in soil monitoring for geophysical purposes. *Radiation Measurements*, 25 (1-4), 547-552, 1995.

- Shapiro, M.H., Rice, A., Mendenhall, M.H., Melvin, J.D., Tombrello, T.A., Recognition of environmentally caused variations in Radon time series. *Pure Appl. Geophys.*, 122, 311-326, 1985.
- Steinitz, G., Begin, Z.B. and Gazit-Yaari, N., A Statistically Significant Relation between Rn Flux and Weak Earthquakes in the Dead Sea Rift Valley. *Geology*, 31, 505-508, 2003.
- Steinitz, G., Martín, M.C., Gazit-Yaari, N., Quesada, M. L., de la Nuez, J., Casillas, R., Malik, U., and Begin, Z.B., Multi-day Radon signals with a radioactive decay limb – occurrence and geophysical significance. *Applied Radiation and Isotopes*, 64/4, 520-524, 2005. DOI: 10.1016/j.apradiso.2005.10.004.
- Steinitz, G., O. Piatibratova, and S. M. Barbosa (2007), Radon daily signals in the Elat Granite, southern Arava, Israel, *J. Geophys. Res.*, 112, B10211, doi:10.1029/2006JB004817
- Steinitz, G., Piatibratova, O., and Malik, U., Radon signals in the Elat Granite pluton, southern Arava, Israel. *Geol. Surv. Rep. GSI/18/06*, 53p., 2006.
- Steinitz, G., Vulkan, U., Lang, B., Gilat, A. and Zafrir, H., Radon emanation along border faults of the Rift in the Dead Sea area. *Israel Jour. Earth Sci.*, 41, 9-20, 1992.
- Steinitz, G., Vulkan, U. and Lang, B., Monitoring of the tectonically related radon flux in Israel. *Isr. Geol. Surv., Current Res.*, 10, 148-153, 1996.
- Steinitz, G., Vulkan, U., Lang, B., The Radon flux at the northwestern segment of the Dead Sea (Dead Sea Rift) and its relation to earthquakes. *Israel Jour. Earth Sci.*, 48, 283-299, 1999.
- Toutain, J. P., Baubron, J. C., Gas geochemistry and seismotectonics: a review. *Tectonophysics*, 304, 1-27, 1999.
- Trique, M., Richon, P., Perrier, F., Avouac, J.P., and Sabroux, J.C., Radon emanation and electric potential variations associated with transient deformation near reservoir lakes, *Nature*, 399, 137-141, 1999.
- Vulkan, U., Assael, Y., Yaffe, Y., Steinitz, G. and Lang, B., 1998. Calibration of detectors used for monitoring Rn in the geological environment. *Isr. Geol. Surv. Rep. TR-GSI/12/98*.
- Weinlich, F. H., Faber, E., Bouskova, A., Horalek, J., Teschner, M., Poggenburg, J., Seismically induced variations in Marianske Lazne fault gas composition in the NW Bohemian swarm quake region, Czech Republic - A continuous gas monitoring. *Tectonophysics*, 421, 89-110, 2006.